ALFRED-WEGENER-INSTITUT
HELMHOLTZ-ZENTRUM FÜR POLAR- UND MEERESFORSCHUNG

Universität Rostock

Potential of Greenland cockles (*Serripes groenlandicus*) as high resolution Arctic climate archive

Potential der Grönlandherzmuschel (*Serripes groenlandicus*) als hochauflösendes Klimaarchiv der Arktis

Masterarbeit im Studiengang Meeresbiologie zur Erlangung des Titels „Master of Science“

Angefertigt von Verena Merk in der Sektion Bentho-Pelagische-Prozesse am Alfred-Wegener-Institut Helmholtz-Zentrum für Polar- und Meeresforschung, Bremerhaven

Matrikelnummer: 212209132
Wohnort: Verdener Str. 29a, 27570 Bremerhaven

Abgabe: 18. März 2015

Erstgutachter: Prof. Dr. Gerhard Graf, Universität Rostock
Zweitgutachter: Dr. Jürgen Laudien, Alfred-Wegener-Institut Helmholtz-Zentrum für Polar- und Meeresforschung, Bremerhaven

Bremerhaven März 2015

Titelbild: G. Veit-Köhler

Zusammenfassung

Um die klimatische Zukunft der Erde vorauszusagen ist das Wissen um ihre Vergangenheit unabdingbar. Klimamodelle, die mögliche Entwicklungen des zukünftigen Klimawandels modellieren, basieren auf Daten früherer Umweltbedingungen. Die Verlässlichkeit dieser Klimamodelle ist abhängig von der Qualität und Quantität dieser Daten. Da Messungen nur begrenzt zur Verfügung stehen werden Klimaarchive herangezogen um die Umweltbedingungen der Vergangenheit zur rekonstruieren. Archive zeichnen, für den Zeitraum ihrer Entstehung, indirekte Informationen über ihre Umgebung auf. Ist die Beziehung zwischen einem, in einem Archiv aufgezeichneten, Stellvertreterparameter und einem Umweltparameter bekannt kann dies als so genannter Proxy verwendet werden. Bivalvien sind möglich Archive, die durch die Veränderungen von Wachstumsraten und Schalencarbonat Zusammensetzungen Rückschlüsse auf das umgebende Meerwasser zulassen. Ein möglicher Proxy ist dabei das Verhältnis von ^{18}O zu ^{16}O ($\delta^{18}O$) Isotopen im Schalencarbonat. Für die meisten Bivalvien ist das Gleichgewicht zwischen $\delta^{18}O$ Werten des Schalencarbonats und des umgebenden Meerwassers abhängig von Temperatur und Salinität. Um die $\delta^{18}O$ Werte des Schalencarbonates einer Muschelart als Proxy nutzen zu können muss die Möglichkeit ausgeschlossen werden, das metabolische Prozess das Gleichgewicht der $\delta^{18}O$ Werte beeinflusst. Dafür müssten $\delta^{18}O$ Werte des Schalencarbonats einer Muschelart mit gemessenen Meerwasserparametern kalibriert werden. Die zirkumpolar Grönlandherzmuschel *Serripes groenlandicus* (Bruguiere, 1789) war bereits in der Vergangenheit Gegenstand stabiler Isotopen Analysen. Jedoch wurde bisher keine Kalibrierung durchgeführt. Die vorliegende Arbeit untersuchte ob die im Schalencarbonat von *S. groenlandicus* gemessenen $\delta^{18}O$ Werte von metabolischen Prozessen beeinflusst werden. Dafür wurden 37 Individuen einer Population in Kongsfjorden (Spitzbergen) entnommen. Die Schalen von drei Individuen wurden zur Analyse stabiler Isotopen herangezogen. Die gemessenen $\delta^{18}O$ Werte der Schale wurden anschließend mit berechneten $\delta^{18}O$ Werten verglichen. Die berechneten $\delta^{18}O$ Werte beruhten auf Temperatur- und Salinitätsmessungen in der direkten Umgebung der *S. groenlandicus* Population. Um zu zeigen, dass die, für die Analyse der stabilen Isotope ausgewählten Individuen repräsentativ für die Population sind, wurden ihre Wachstumsraten mit den der ebenfalls gesammelten Individuen verglichen. Zudem wurde festgehalten zu welchem Zeitpunkt die Muscheln dunklere Inkremente (Wachstumslinien) in ihre Schale einbauen. Mit Hilfe eines Konfokalen Raman Mikroskops und eines Rasterelektronenmikroskops wurde die Struktur des Schalencarbonates überprüft. Die Ergebnisse zeigen, dass die Wachstumsraten aller gesammelten Individuen vergleichbar waren. Die Überprüfung der Wachstumslinien ergab, dass diese im Spätsommer bis Herbst gebildet wurden. Es konnte außerdem gezeigt werden, dass die Schalenstruktur von *S. groenlandicus* aragonitisch ist. Allerdings zeigte sich an manchen Stellen auch eine erhöhte Porosität. Die Analyse stabiler Sauerstoff Isotope des Schalencarbonates ergab, dass eine große Ähnlichkeit zwischen gemessenen und berechneten $\delta^{18}O$ Werten gab. Berechnete Minimalwerte wurden dabei nicht in der Schale aufgezeichnet. Die lässt vermuten, dass das Wachstum von *S. groenlandicus* entweder von höheren Temperaturen oder geringer Salinität gehemmt wurde. Aus diesen Ergebnissen wurde geschlossen, dass das Gleichgewicht zwischen $\delta^{18}O$ Werten des Meerwassers und des Schalencarbonates nicht durch metabolischen Prozesse beeinflusst wird. Zusätzlich war es möglich die Schalen durch manuelles fräßen der Proben hochauflösend zu beproben (65μm).

Abstract

In order to predict the climatic future of the earth, knowledge about the past is indispensable. Climate models which predict possible developments of future climate change are based on data of past environmental conditions. The precision of these climate models depends on quality and quantity of those data. Since recent measurements are limited, climate archives are used to reconstruct past conditions. Archives indirectly provide information about the surrounding environmental conditions at the time of their formation. Once the relationship between a representative parameter recorded by an archive and an environmental parameter is known this could function as a so called proxy. Bivalves are possible archives recording ambient seawater parameter incrementally as a variation of growth rates or shell calcium carbonate ($CaCO_3$) composition. A potential temperature proxy is the ratio of $^{18}O/^{16}O$ ($\delta^{18}O$) recoded in the shell carbonate of some Bivalves. The equilibrium between recoded and measured $\delta^{18}O$ of the seawater is determined by temperature and salinity. In order to use this recording of $\delta^{18}O$ in shell carbonate it is necessary calibrating $\delta^{18}O$ of the seawater with measurements of surrounding seawater parameters to exclude the possibility of metabolic influences on this equilibrium. The Greenland cockle *Serripes groenlandicus* (Bruguiere, 1789), a bivalve occurring circumpolar has already been a subject to stable oxygen and carbon isotopes analyses. However, a calibration have not been provided yet. This study investigated whether the equilibrium between $\delta^{18}O$ measured subsequently in shell carbonate of *S. groenlandicus* and the ambient seawater is influenced by metabolic processes. Therefor the shells of 37 specimens, were collected from a population located in Kongsfjorden (Spitsbergen). Three of them were used to subsequently measure $\delta^{18}O$ values of shell carbonate and compared to predicted $\delta^{18}O$ shell values. The predicted $\delta^{18}O$ values of the shell were calculated from temperature and salinity measurements of the ambient seawater. Growth line deposition and growth rate were examined in specimens of the same population in order to prove that the three individuals chosen for stable isotope analysis are representative for this population regarding their growth pattern. Additionally the structure of shell carbonate was analyzed using a Confocal Raman microscope and a scatter electron microscope. Results prove, that the individuals chosen for stable isotopes analyses were representative individuals of the population regarding their growth rate. The evaluation of growth line deposition examined in all collected shells showed a deposition in late summer up to fall. It was also proven that the crystalline structure of the shell carbonate was aragonite. However, embedding shells in Araldite showed the occurrence of a porous structures in the outer shell layer. Stable oxygen isotope analysis and comparison with ambient conditions during shell formation prove a strong similarity between predicted and measured $\delta^{18}O$ values of the shell where an alignment was possible. However, the minimum of predicted $\delta^{18}O$ values was not recoded in the shell carbonate, indicating that the growth of *S. groenlandicus* is limited by either high temperature or low salinity. The total range of $\delta^{18}O_{shell}$ values was 3.53‰. From these findings it was concluded, that the equilibrium between shell stable oxygen isotope ratios is not influence by metabolic processes. It was furthermore noted that a high resolution sampling (68 μm) of shell carbonate of *S. groenlandicus* by manual milling possible.

Content

Zusammenfassung ..... **I**
Abstract ..... **II**
Abbreviations and acronyms ..... **V**
List of Tables ..... **VI**
List of Figures ..... **VI**
1 Introduction **1**
2 Objectives **6**
3 Materials and methods **7**
3.1 Study site **7**
3.2 Shell collection and environmental data **9**
3.3 Shell preparation **10**
3.4 Representativeness of individual growth **11**
3.4.1 Growth line deposition 11
3.4.2 Growth rate 13
3.5 Crytalline structure of the shell carbonate **14**
3.5.1 Confocal Raman microscopy 14
3.5.2 Electron microscopy 16
3.6 Stable oxygen and carbon isotopes **17**
3.6.1 Sampling of biogenic calcium carbonate of shells 17
3.6.2 Measurment of stable oxygen and carbon isotopes 19
3.6.3 Alignment of measured and calculated $\delta^{18}O$ values 19
4 Results **21**
4.1 Representativeness of individual growth **21**
4.1.1 Growth line deposition 21
4.1.2 Growth rate 22
4.2 Crystalline structure of the shell carbonate **24**
4.2.1 Confocal Raman microscopy 24
4.2.2 Electron microscopy 27
4.3 High resolution sampling of calcium carbonate **29**
4.4 Oxygen and carbon stable isotopes **29**

5 Discussion 35
5.1 Representativeness of individual growth 35
5.2 Crystalline structure of the shell carbonate 35
5.3 High resolution sampling of calcium carbonate 36
5.4 Oxygen and carbon stable isotopes 37
6 Conclusion and outlook 39
7 References 40
8 Declaration 44
9 Acknowledgment 45

Abbreviations and acronyms

δ	Delta
$\delta^{13}C$	Stable carbon isotope ratio of ^{13}C to ^{12}C
$\delta^{18}O$	Stable oxygen isotope ratio of ^{18}O and ^{16}O
$\delta^{18}O_{predicted}$	Predicted stable oxygen isotope ratio of the shell carbonate
$\delta^{18}O_s$	Stable oxygen isotope ratio influenced by salinity
$\delta^{18}O_{shell}$	Stable oxygen isotope ratio of the shell carbonate
^{12}C	Stable isotope of carbon with 12 neutrons
^{13}C	Stable isotope of carbon with 13 neutrons
^{18}O	Stable isotope of oxygen with 18 neutrons
^{16}O	Stable isotope of oxygen with 16 neutrons
a	Year
ArW	Arctic Water
AWI	Alfred-Wegener-Institut Helmholtz-Zentrum für Polar- und Meeresforschung
C	Carbon
$CaCO_3$	Calcium carbonate
CO_2	Carbon dioxide
CRM	Confocal Raman microscopy
DOG	Direction of growth
e.g.	exempli gratia, Latin for “for example”
et al.	et alii, Latin for “and others”
IPCC	Intergovernmental Panel on Climate Change
IRMS	Isotope ratio mass spectrometer
k	Growth constant
NAO	North Atlantic Oscillation
O	Oxygen
pH	Negative logarithm of the hydrogen ion concentration
R^2	Error square
S. groenlandicus	*Serripes groenlandicus*
SEM	scattering electron microscope
SH_∞	Asymptotic maximum shell height
SH_t	Shell height at time t
S_{sea}	Salinity of the seawater
t	Time in years
t_0	Time when shell height was theoretically zero
T_{sea}	Temperature of the seawater
VPDB	Vienna Peedee Belemnite
WSC	West Spitsbergen Current

List of Tables

Table 1. Verification of the calcein lines, differentiated between umbo and shell. 21
Table 2. *S. groenlandicus*: List of carbonate samples taken from three shells. 29

List of Figures

Figure 1: Overview of the shell morphology of the Greenland cockle *S. groenlandicus* 5
Figure 2: Map of Spitsbergen and the Kongsfjorden-Krossfjorden system..... 8
Figure 3: Enclosure (3 x 3 m) where the population of Greenland cockles was held.....10
Figure 4: Incubation of Greenland cockles in 100 mg l-1 calcein solution. 11
Figure 5: Examples for calcein lines under reflected and fluorescent lights 12
Figure 6: *S. groenlandicus:* Measurement of the width of two increments using AnalySIS 5.0 software. 13
Figure 7: Rayleigh and Raman scattering.....15
Figure 8: Sampling of calcium carbonate for stable isotopes analysis 18
Figure 9: Number of increments per year and ontogenetic shell age. 23
Figure 10: Shell height-at-age data for the shell taken for the *S. groenlandicus* sub-population, including von Bertalanffy growth function 23
Figure 11: Confocal Raman microscopy map and spectrum of shell cross sections of *S. groenlandicus*. 24
Figure 12: Different images of the shell structure of *S. groenlandicus* 26
Figure 13: CRM spectra of a region with 'spots'.....27
Figure 14: Scanning electron microscope images showing cross sectioned shell of *S. groenlandicus*.....28
Figure 15: $\delta^{18}O_{shell}$ values for all three individuals displayed with equal spacing 31
Figure 16: Seawater temperature, salinity and $\delta^{18}O_{predicted}$ at the study site 32
Figure 17: Alignment of δ^{18}Oshell and $\delta^{18}O_{predicted}$ values.....33
Figure 18: δ^{13}C values of shell carbonate taken from *S. groenlandicus* shells 34

1 Introduction

Throughout the 4.5 billion years of its existence the earth experienced a broad variety of changes, including changes in the composition of the atmosphere (Catling and Claire 2005), the origin and evolution of life (Baross and Hoffman 1985) and the movement of continents related to plate tectonics (Wegener 1912). Furthermore, extensive variations in climatic conditions let to transitions between glacial and interglacial periods (e.g. Rogers 1993). The understanding of how and why global and local climatic conditions changed in the past provides the possibility to understand and identify the major forces involved in this process (IPCC 2013). Additionally, by looking at the past we can predict how the biosphere and coupled mechanisms may react to a specific change in the climate system. The polar regions in particular reacts very sensitive to such variations due to polar amplification. Meaning the melting of snow and ice exposes ocean and land surfaces that absorb solar radiation much more effective. Thus they will heat up causing further melt of ice and snow which again would expose more ocean and land surfaces. The Arctic in particular is more sensitive than the Antarctic since its temperatures are near to the melting point (Miller *et al.* 2010; Serreze and Francis 2006)

The knowledge about environmental conditions of the past (e.g. climate) is based on data such as ocean and land temperature, salinity and pH of seawater. Since recent measurements are limited in times they are combined with reconstructed data to verify climate models. Those climate models can for instance be used to predict the anthropogenic induced climate change the earth is about to face in the near future (IPCC 2013).

Climate models are numerical models, which intend to predict the future development of important environmental parameters (e.g. global temperatures) based on various assumptions such as the future anthropogenic emissions of carbon dioxide (CO_2). Their precision relays on the comparison to modeled past conditions with reconstructed (proxy data) or measured parameters. Furthermore, the accuracy depends on quality and the temporal resolution of the reconstructed and measured data. The better the amount, continuity, resolution and certainty of the data available, the better the reliability of the climate model (Fischer and Wefer 1999; IPCC 2013).

In order to reconstruct past environmental and climatic conditions many different archives and proxy data are used. Archives indirectly provide information about the surrounding environmental conditions. At the time of growth or deposition different archives can indirectly record distinct environmental parameters, such as temperature or salinity (Versteegh *et al.* 2012). Once a correlation between such a representative parameter (proxy) and an environmental condition is identified and understood, this proxy can be used to reconstruct

paleo-climatic or -environmental information. Since different archives provide data in spatially and temporally limited ranges, data sets need to be complementary. Archives can be biogenic such as bivalves, trees, corals, coralline algae, fish otoliths and or non-biogenic such as the composition of ice or sediments cores (e.g. Fischer and Wefer 1999; IPCC 2013). Environmental information archived through biogenic proxies can be retrieved from the variability of growth patterns (e.g. annual growth rates of bivalves) or the biogeochemical composition of bio-minerals (e.g. stable isotope ratios or trace and minor elemental ratios from shell carbonate) (Fischer and Wefer 1999).

All physical and chemical studies of incrementally and chronological features in biological hard tissue of marine and freshwater organisms can be referred to as sclerochronology (Jones 1983). Organisms known to grow discrete are bivalves (e.g. Richardson 2001). Since their shell growth is asymptotic they record environmental conditions over their whole lifespan (Richardson 2001). Bivalves grow by secreting calcium carbonate ($CaCO_3$) and thus extending their shell towards the ventral margin (Richardson 2001). Most shells follow a pattern of alternating lighter and darker bands, which may be prominent in cross sections, as well as on the outer shell surface (Richardson 2001). In many bivalve species the thinner, but darker bands or growth lines are known to form annually (e.g. Ambrose *et al*. 2006; Bušelić *et al*. 2014). Due to unfavorable conditions, such as low water temperatures or a lack of food, the shell secreting mantle edges are retracted from the margins (Richardson 2001). As a consequence growth slows down or stops (Richardson 2001). Once it has been proven that the darker growth lines are built annually they can be used for age determinations. If conditions are more favorable shells grow at a higher rate (Richardson 2001). This results in wider and lighter increments, which are built gradually over the growth period. The overall annual growth of bivalves is determined by their biology, the ontogenetic age and environmental conditions such as temperature and nutrient supply (Jones *et al*. 1989; Schöne 2013). In general, more favorable conditions lead to wider annual increments. This concept was used extensively in standardized growth models to correlate shell growth with environmental events (Ambrose *et al*. 2006; Bušelić *et al*. 2014; Schöne 2008). Once established, such a correlation can be used as a proxy to reconstruct past environmental conditions for selected geographic regions (Marchitto *et al*. 2000).

Despite using morphological features it is also possible to receive information from the shell material itself. The biogeochemical composition of the shell carbonate is determined by a variety of physical and chemical properties of the ambient seawater. Thus, stable isotope geochemistry is implemented frequently in paleontological studies (Wassenaar, Brand, and Terasmae 1988). In order to use stable isotope ratios for the reconstruction of ambient

conditions, the influences of different parameters such as seawater temperature, salinity or metabolic processes of the organism need to be understood (Schöne 2008).

Stable carbon isotope ratios ($\delta^{13}C$) potentially contain information about water properties related to primary production. However, the biological influence on its incorporation into the shell carbonate is not yet fully understood and therefore it is not possible to reliably interpret them (for details on $\delta^{13}C$ in bivalves see Gillikin *et al*. 2007; Romanek *et al*. 1992).

In contrast, for the stable oxygen isotopic composition much is already known about the mechanisms (e.g. Epstein and Mayeda 1953). As the ratio of $^{18}O/^{16}O$ ($\delta^{18}O$) is inversely linked to temperature (Epstein *et al*. 1961) changes in the ratio of ^{18}O to ^{16}O is theoretically mainly caused by thermodynamic processes. The changes in the ration of ^{18}O to ^{16}O is referred to as fractionation.

In reality this fractionation is much more complex, especially in marine environments. Evaporation effects $\delta^{18}O$ since the lighter ^{16}O is more likely to change into vapor phase (Epstein and Mayeda 1953). Conversely, ^{18}O is more prominent in precipitation. An additional factor in marine environment is the difference between seawater and freshwater. In general, changes in salinity affect $\delta^{18}O$ in similar ways but not equally pronounced (Epstein and Mayeda 1953). The $\delta^{18}O$ values of freshwater are much lower and they also differ between sources. The $\delta^{18}O$ values of for example melted snow are much more negative than the values of a river inflow not fed by meltwater. Thus the negative influence of an inflow fed by meltwater on the $\delta^{18}O$ of seawater is higher, than the one cause by a river inflow not fed by meltwater, however, both events will lower salinity likewise (Epstein and Mayeda 1953). This leads to ocean waters with the same salinity, but different $\delta^{18}O$ (Epstein and Mayeda 1953). In order to work with the relationship between salinity and $\delta^{18}O$ it is necessary to determine it for each study area (Maclachlan *et al*. 2007).

The real paleontological value of variations in stable oxygen isotope compositions is based on the knowledge of how they are incorporated into the biogenic carbonate. Without any metabolic inference the incorporation into the shell carbonate is in equilibrium with the ambient $\delta^{18}O$ of the seawater. This relationship however depends on the polymorphs of calcium carbonate (for bivalves mostly calcite or aragonite) (Epstein and Mayeda 1953; Grossman and Ku 1986). Once proofed for a particular species, that there are no metabolic processes influencing the $\delta^{18}O$ it can be used as a temperature proxy wherever $\delta^{18}O$ of the seawater or its correlation with salinity is known (Schöne and Fiebig 2009).

In the past this approach has been used for different calcifying organisms such as bivalves or calcifying foraminifera (Versteegh *et al*. 2012; Zachos *et al.* 1996). However, some bivalves have, despite a long lifetime and global distribution one crucial advantage: The incremental shell accretion allows for an examination of the variation in carbonate composition on an intra-

annual scale (Richardson 2001). This enables the possibility to resolve seasonal patterns within the shell (Hallmann *et al*. 2008, 2009; Khim *et al.* 2001; Versteegh *et al*. 2012).

Khim (2002) and Khim *et al.* (2003) used shells of the Greenland cockle *Serripes groenlandicus* (Bruguiere, 1789) to reconstruct seawater temperatures and salinity of seawater. He concluded that there are no metabolic changes to the stable oxygen isotope incorporation by the animal. However, for the potential Arctic bio-archive *S. groenlandicus* this proof and calibration have not yet been provided directly.

S. groenlandicus is an infaunal suspension feeder. Populations of this cockle occur circumpolar in the Arctic up to the boreal regions and can be found from the subtidal zone down to 100 m water depth (Khim 2001; Kilada *et al.* 2007). In recent years this cockle species became a valuable by-catch in the fishery of the Arctic surfcalm (*Mactromeris polynyma*) in Canada (Kilada *et al*. 2007). Unlike some other bivalve species *S. groenlandicus* is able to move and change its location or even escape from predators (Legault and Himmelman 1993). Like most representatives of the family Cardiidae, they have a three-layered shell-structure consistent of the interior layer and middle layer (ostracum) **(**Figure 1) and an outer layer of organic conchiolin, the periostracum. It is known, that the deposition of dark growth lines occurs annually in late summer to early fall (Ambrose *et al*. 2006). This makes them suitable for sclerochronological studies. Analysis of growth rates showed that there is a possible correspondence to the Arctic Climate Regime Index (ACRI, Ambrose *et al*. 2006; Carroll *et al*. 2011). With a maximum length of 100 mm and a maximum ontogenetic age of 39 years (Khim 2001; Kilada, Roddick *et al.* 2007), they are suited for providing high-resolution environmental data covering a long (multi-decadal) time period. The species reaches its maximum growth rate at the age of nine with an annual shell growth peak in July followed by a sharp drop in August (Kilada *et al*. 2007). Knowledge about their reproduction is limited. So far it is known that they are hermaphroditic with their male tissues reaching sexual maturity at an age of 2.83 years and female tissue at 3.69 years (Kilada *et al*. 2007). Studies analyzing spawning are not available.

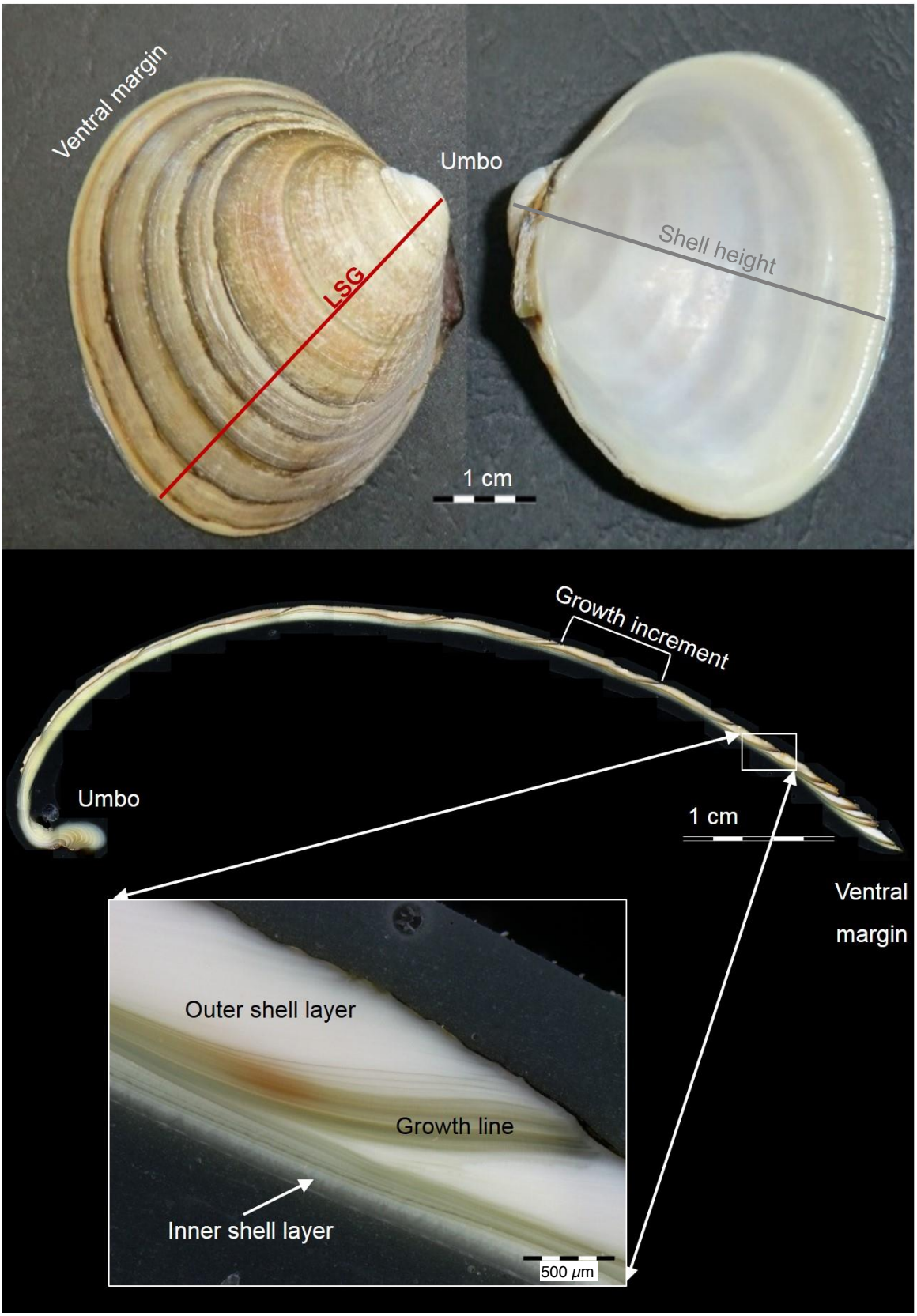

Figure 1: Overview of the shell morphology of the Greenland cockle *S. groenlandicus.* Top: Inner and outer view of the left shell. Red line marks the line of strongest growth (LSG) from the umbo to the ventral margin perpendicular to the growth lines. Grey line marks the measuring line for shell height. Bottom: Cross section following the LSG. Magnified is the area around a growth line, showing the inner and outer shell layer.

2 Objectives

The overall goal of this study is to evaluate the potential of Greenland cockle *S. groenlandicus* as a high resolution climate archive for the Arctic. For this purpose a calibration between $\delta^{18}O$ values measured in shell carbonate and calculated $\delta^{18}O$ shell values (based on measurements of the ambient seawater temperature and salinity) will be applied. Since the number of individuals used for stable isotope analysis will be limited, it is necessary to ensure that the growth patterns of the analyzed shells does not differ from other individuals of the same population. Therefore an analysis of annual shell size increase and an evaluation of the timing of growth line deposition will be carried out. Additionally, the feasibility of high resolution shell carbonate sampling needs to be verified, as well as the suitability of the shell carbonate for analyzing stable isotopes.

3 Materials and methods

3.1 Study site

Kongsfjorden is located on the northwest coast of the Svalbard Archipelago, a group of Arctic islands (Figure 2). It is part of the two-armed fjord system Kongsfjorden-Krossfjorden system, which is linked to the Atlantic Ocean via a deep glacial basin, Kongsfjorddrenna (Figure 2). The course of Kongsfjorden goes from south-east to north-west over a length of 20 km and a width of 4 to 10 km (Svendsen *et al*. 2002). It may be divided into several basins, an outer basin with an average water depth of 200 – 300 m (maximal 429 m) and a distinctly shallower inner basin with a maximal depth of 94 m (on average 50 – 60 m) (Wlodarska-Kowalczuk and Pearson 2003).

Oceanographic conditions of Svalbard are influenced by two major currents (Figure 2): The West Spitsbergen Current (WSC) and the Arctic Water (ArW). The cold and fresh ArW is flowing from the Barents Sea along the east coast of Spitsbergen to the south. At the southern tip it merges with the WSC and heads towards the North. The WSC is the most northern extension of the Norwegian Atlantic Current. It transports huge amounts of heat and salt along the western shelf slope to the North. The temperature and salinity of waters west of Spitsbergen are strongly affected by the seasonal and annual fluctuations of the WSC. The WSC is mainly influenced by the North Atlantic Oscillation (NAO), which is the result of the variability in the pressure ratios between the Azores High and the Icelandic Low (Cottier *et al*. 2005; Hop *et al*. 2002; Schauer *et al*. 2004; Svendsen *et al*. 2002). Further, various sources of fresh water have a big impact on the oceanographic conditions in Kongsfjorden (Svendsen *et al*. 2002). The major input of fresh water are the four tidewater glaciers draining into the fjord (Svendsen *et al*. 2002). Additionally fresh water derives also from snowmelt, precipitation, river run-off and groundwater discharge (Cottier *et al*. 2005). Svendsen *et al.* (2002) estimated the annual discharge of fresh water to be about 1.4 km^3 (annual variation up to 30 %).

Draining of the tidewater glaciers also carries a significant amount of terrestrial sediment (Elverhødi and Seland 1983). The sedimentation rates decline with increasing distance to the glaciers. The rate varies between 20,000 $g \times m^{-2} \times a^{-1}$ at the glacier front to 1,800 – 3,800 $g \times m^{-2} \times a^{-1}$ in the central part of the fjord and down to 200 $g \times m^{-2} \times a^{-1}$ at the entrance of the fjord (Svendsen *et al*. 2002).

Considering the two different currents and the seasonal modification in oceanographic conditions affecting Kongsfjorden it is usually addressed as a border area between Atlantic and Arctic biogeographic zone with a precipitous gradient in sedimentation and salinity (Hop *et al*. 2002). This causes a reduction in biomass and benthic community diversity in the inner

fjord. Along this gradient a mixture of boreal and Arctic marine flora and fauna can be found (Hop *et al*. 2002).

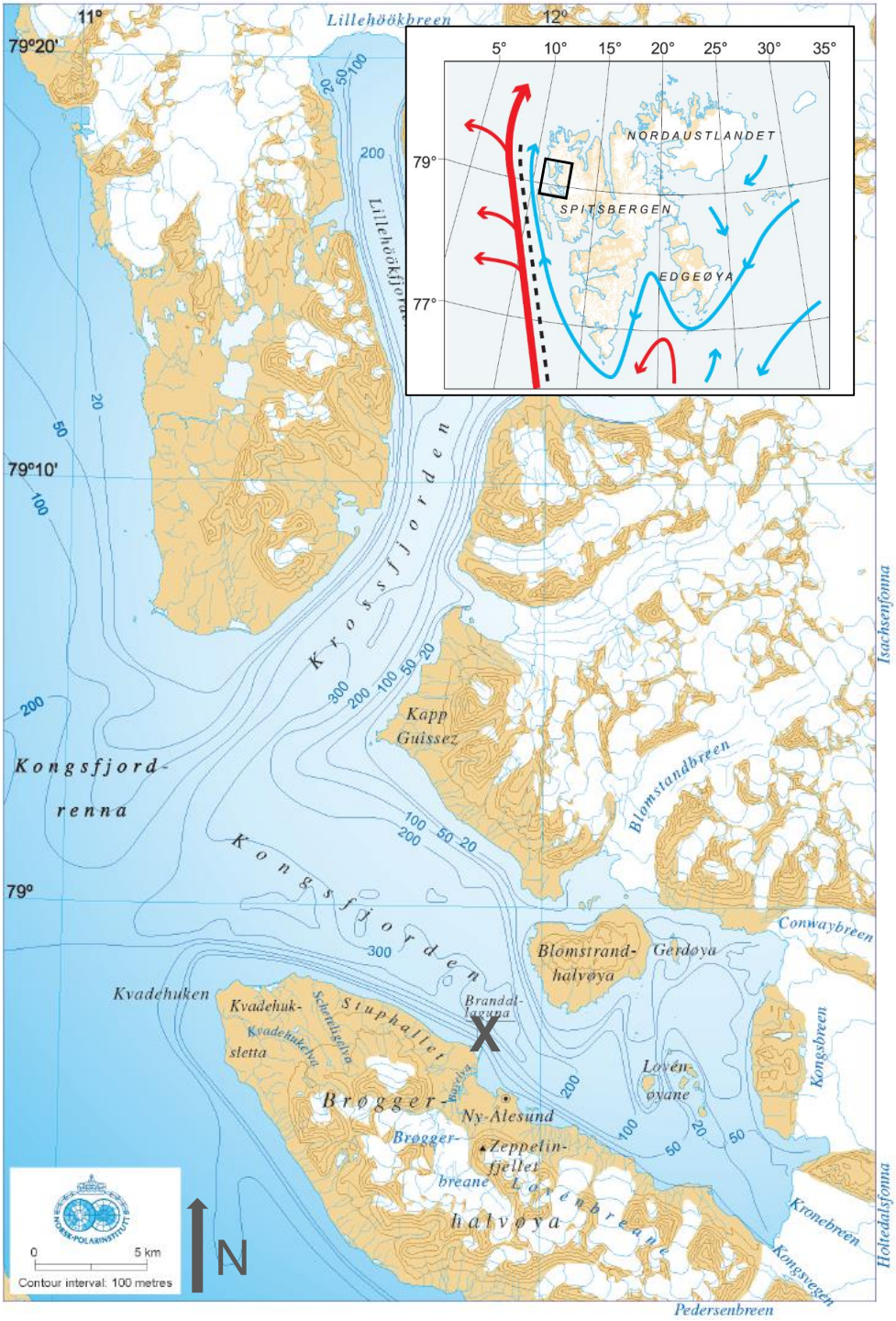

Figure 2: Map of Spitsbergen and the Kongsfjorden-Krossfjorden system. The black cross marks the sampling location Brandal (78°56'52.08''N, 11°51'9.54''E). Upper right corner: Overview of the Spitsbergen archipelago highlighting the major currents: West Spitsbergen Current (red line) and Arctic water (blue line). Kongsfjorden is located within the square (adjusted from Svendsen *et al*. 2002).

3.2 Shell collection and environmental data

The cockles used for this study were caged in an enclosure on the seafloor in order to retrieve them every year for treatment (Figure 3). Additionally water temperature and salinity were recorded at this site.

The position for the setup was situated near the shore in a water depth of 9 m (Brandal, 78°56'52.08''N, 11°51'9.54''E). The enclosure covered a field of 3 x 3 m (Figure 3). Its extent into the sediment was about 30 cm. The sub-population of Greenland cockles contained in the enclosure was collected in its near surroundings. On an annual basis all cockles thriving in the enclosure were marked mechanically with a small notch from the perpendicular on ventral shell margin up on one shell side. For this an electric underwater rotary drill (Dremel 8200 12VMax, Racine, WI, USA) sealed in a custom-made underwater housing and equipped with one or two cut-off wheel (Dremel cut-off wheel No. 409, Ø 24 mm, 0.6 mm thick) was used (Laudien, Brey, and Arntz 2003). The number of individuals within the enclosure was kept stable by replacing gathered cockles. The enclosure was cleaned from colonizing and entrapped drifting macroalgae at least once a year.

To continuously record water temperature and salinity a combined temperature and conductivity logger (μS-Log540, Driesen + Kern GmbH, Bad Bramstedt, Germany) was used. The sensors were located approximately 1.5 m away from the enclosure and about 25 cm above the seafloor. The logger was mounted to a rod and covered with a black plastic cylinder, which was open at the lower end. It recorded the data in intervals of 10 min from September 2009 until September 2014 (Laudien 2011, 2013). Due to a technical malfunction data from June 2011 to September 2012 was not recorded.

Figure 3: Enclosure (3 x 3 m) where the population of Greenland cockles was held. Exact location of the enclosure can be seen in Figure 2. (Photo: M. Schwanitz)

3.3 Shell preparation

In total 40 representatives individuals of *S. groenlandicus* were re-collected in 2012 and 10 individuals in 2014. Individuals were dissected, the shells separated from the respective soft tissue, and thereafter cleaned with a toothbrush before air-drying. Subsequently all shells used in this study were cross sectioned. In order to prepare a cross section along the line of strongest growth (LSG; see Figure 1) the shell has been stabilized using a two-compounded metal-epoxy resin (1:1 ratio; WIKO EPOXY METALL; GLUETEC, Greußheim, Germany). It was applied on the inside and outside of the shell, following the LSG from the umbo to the margin in a ca. two centimeters wide coat. The resin was left to dry for 12 hours at room temperature. Thereafter the shells were cut with a circular saw bench (FKS/E; Proxxon, Föhren, Germany) and a diamond coated cutting blade (blade: NO 28 735; Proxxon, Föhren, Germany). The sectional surface was grinded until the growth lines became visible, utilizing a manual grinder (Phoenix Alpha; Buehler, Düsseldorf, Germany) and abrasive paper (grain sizes: 25 μm, 15 μm, 10 μm and 5 μm). For stability reasons the shell halves without the notch were selected, therefore it was not possible to use always the same shell valve.

3.4 Representativeness of individual growth

The population structure was examined regarding general growth parameters such as the timing of growth line deposition and growth rate.

3.4.1 Growth line deposition

The time of growth line deposition was determined by a mark and recapture approach. In the years 2008, 2009 and 2011 shells were labelled with calcein (Merck; Darmstadt, Germany) following Herrmann *et al*. (2009) and Riascos *et al*. (2007). The incubation with 100 mg l^{-1} calcein solution took place in aerated seawater in a cold room for three hours (Figure 4). This procedure resulted in clearly visible fluorescent lines without any mortality.

Calcein lines were viewed in the cross sections using a fluorescence light source (Model U-ULS100HG, Olympus, Hamburg, Germany) attached to a microscope (Research Stereomicroscope System SZX12, Olympus, Hamburg, Germany). The shell as well as the umbo was examined (Figure 5). Pictures were taken using a digital camera mounted to the microscope (CCD-camera U-CMAD3 Colorview I; Olympus, Hamburg, Germany) and a supplementary image analysis software (AnalySIS 5.0 Copyright 1986-2004; Soft Imaging System GmbH, Olympus, Hamburg, Germany).

Figure 4: Incubation of Greenland cockles in 100 mg l^{-1} calcein solution. Visible are several Greenland cockles with extended siphons. (Photo: G. Veit-Köhler)

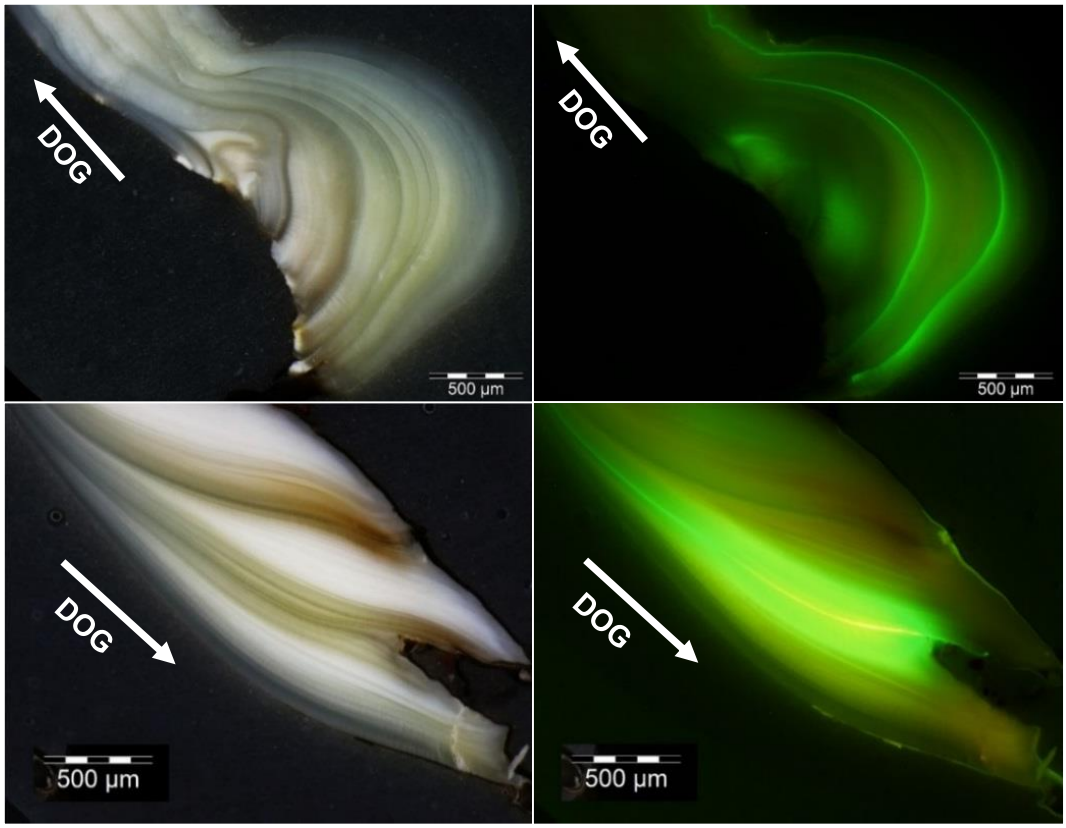

Figure 5: Examples for calcein lines under reflected (left hand side) and fluorescent lights (Right hand side). Green lines visible under fluorescent lights in the umbo (top) and shell increment (bottom) are calcein lines. Positions of calcein lines were detected by comparison with pictures taken under reflected lights.

3.4.2 Growth rate

For describing the growth rate of *S. groenlandicus* the widths of their increments were measured. These increments represent the annual increase in shell size and allow the modelling of a growth function.

The measurement of increment widths was performed using a video-imaging-system (see Section 3.4.1). The shells were fixated with periphery wax (Surgiden, Handewitt, Germany) onto a glass-slide (76 x 26 mm) in order to achieve and maintain a parallel plane between the camera and the cross section. Measuring started at the first dark growth line visible in the ontogenetically youngest part of the shell. The first increment was excluded to define a clear and unified starting point for all shells.

An increment was defined as the distance from the end of one dark growth line to the end of the next dark growth line in direction of growth (DOG) (Figure 6). In order to minimize systematic errors, the means of three measurements of the same increment were calculated. The last increment of each shell was excluded since it was still under development at time of sampling.

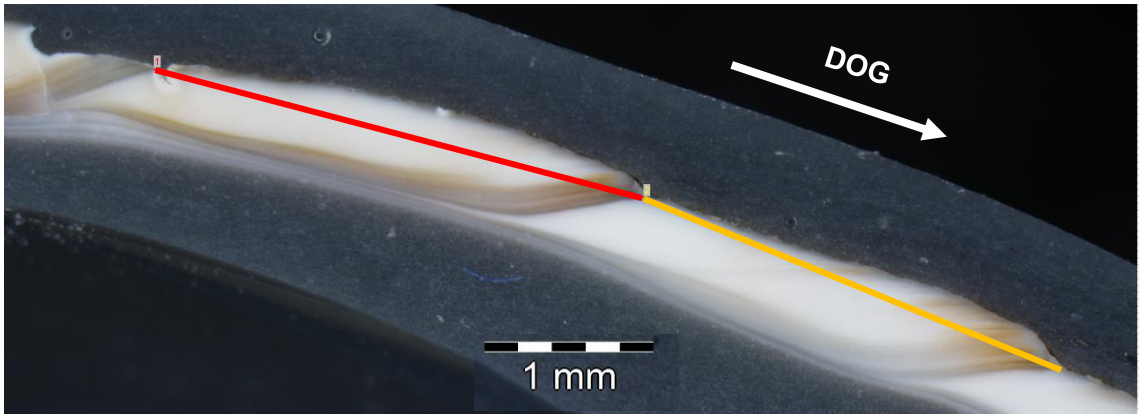

Figure 6: *S. groenlandicus*: Measurement of the width of two increments using AnalySIS 5.0 software. Width of increments was measured from the end of one growth line to the end of the next in direction of growth (DOG). Red line indicates ontogenetic year one, while the yellow line indicates ontogenetic year two.

Shell growth was modeled by fitting a von Bertalanffy growth function to the shell height-at-age data using a nonlinear algorithm (Equation 1, von Bertalanffy 1957). The fitting process was done iterative by minimizing the error square using the excel-solver (Microsoft® Office 2013) (Laudien *et al.* 2003). Main purpose was to compare the growth rates of the individuals taken for the stable isotope analysis to the growth rates of the entire population.

$$SH_t = SH_\infty * (1 - exp\ (-k\ (t - t_0)) \quad \textbf{Equation (1)}$$

With:	SH_t	–	Shell height at time t
	SH_∞	–	Asymptotic maximum shell height
	k	–	Growth constant
	t	–	Time in years
	t_0	–	Time when shell heigt was theoretically zero

3.5 Crystalline structure of the shell carbonate

The crystalline structure of the biogenic calcium carbonate was analyzed using a Confocal Raman microscope (CRM). To get further information on the crystalline structure shells were also examined using a scattering electron microscope (SEM).

3.5.1 Confocal Raman microscopy

Light interacts with molecules in three different ways. First by passing through, second by getting absorbed and third by being scattered. The Confocal Raman microscopy is based on the scattering of photons. Like absorption, scattering occurs when a photon hits a molecule and promotes this molecule to a higher energetic state. Unlike absorption, the scattered photon, which is emitted by the molecule when falling back to a lower energetic state, radiates in a modified angle to the incoming laser. Additionally scattering does not require the incident frequency to match the difference between the two states of the molecule. This is due to the fact that scattering distorts (polarizes) the cloud of electrons around the nuclei, not like absorption promoting an electron to a higher state. The energy state created by distorting the electron cloud is determined by the frequency of the photon (Smith and Dent 2005).

The majority of the light scatters elastically (Rayleigh scattering). Only a few photons are scattered inelastically (Raman scattering, Figure 7). Rayleigh scattering occurs when only the cloud of electrons is involved and no measurable energy is transferred between photon and molecule. The scattered photon has the same frequency as the one emitted by the laser. A Raman scattering includes an effect on the nucleus, causing energy to transfer from the photon to the molecule (Stoke scattering). The molecule gets promoted from the ground state “m” to a higher energetic state and by emitting a photon falls to the slightly excited state “n”. The scattered photon has a different frequency as the incident. This shift in energy (Stokes shift) is molecule specific. The natural occurrence of this slightly exited state of a molecule is determined by temperature. When irradiated with a laser it will cause an energy transfer from

the molecule to the photon, an Anti-Stoke scattering. The change in energy state of the molecule also matches the Stokes shift. The Confocal Raman microscope measures the frequency differences between the laser and the scattered light and thus the Stokes shift (Smith and Dent 2005). These measured spectra of frequency peaks are specific for each mineral and mineral polymorph. In case of biogenic calcium carbonate it can e.g. be used to distinguish between calcite and aragonite (e.g. Nehrke and Nouet 2011)

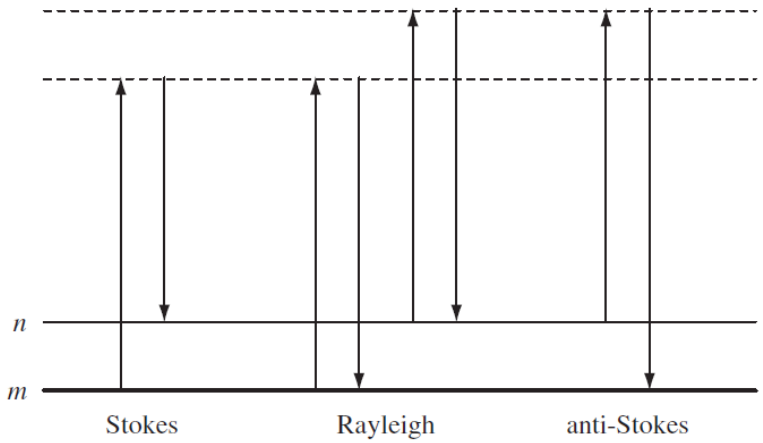

Figure 7: Rayleigh and Raman scattering. Raman scattering differentiated in Stokes and anti-Stokes scattering. Energetic ground state “m” at the bottom, slightly excited state “n” above it. High energetic states at the top (Smith and Dent 2005).

For CRM analysis the shells needed to be embedded into Araldite®, a fluid epoxy resin (Araldite®2020, Huntsman, Bad Säckingen, Germany) since this is not so like to get burned by the laser as the previously used metal-epoxy.

Four shells were embedded in Araldite without further preparation (shell IDs: 27ASGkofj2012, 01-, 03-, 05ASGkofj2014). In order to get rid of the periostracum and organic residues one shell (shell ID: 10ASGkofj2012) was previously submerged in 13 % sodium hypochlorite-solution for 10 min. Two shells were already coated with metal-epoxy resin (see Section 3.3) and previously cross sectioned. After removing the metal-epoxy resin from the outer side of the shell they were embedded in Araldite (shell IDs: 17-, 25ASGkofj2014).

Embedment of the shells with Araldite took place in a small container built from aluminium foil. It was internally coated with a release agent (Nr. 20-8185-002, Buehler, Düsseldorf, Germany) to prevent the Araldite from sticking to it. First the ground of the container was covered with a thin layer of epoxy. Either the shell was put cross section downwards or as a whole shell valve, inner side up into the container. Afterwards the shell was covered completely with Araldite. The embedding was left to dry for 24 h. In case the entire shell was embedded a low-speed precision saw (IsoMet, Buehler, Düsseldorf, Germany) with a 0.4 mm diamond-

coated saw blade was utilized to cut along the LSG. Embedded cross sections were ground using a manual grinder (Phoenix Alpha; Buehler, Düsseldorf) and abrasive paper (grain sizes: 25 μm, 15 μm, 10 μm and 5 μm) until the growth line was visible. In case the shell was already cross sectioned it was grounded until no Araldite was covering the cross section any longer.

For analysis a Confocal Raman microscope (alpha 300 R; WITec, Ulm, Germany) and a monochromatic light sources with a wavelength of 488 nm and a 20× objectives (EC Epiplan, NA = 0.4; Zeiss, Oberkochen, Germany) was used. Signals were detected using a UHTS300 ultra high throughput spectrometer (WITec GmbH, Ulm, Germany) and processed with WItec Project FOUR (WITec GmbH, Ulm, Germany).

3.5.2 Electron microscopy

In order to have a check for porosity in the carbonate two shell cross sections were analyzed utilizing a scattering electron microscope (Quanta FEG 200; FEI, Oregon, USA). One of the shells was coated with metal-epoxy (see Section 3.3). One has been embedded in Araldite (see Section 3.5.1). SEMs produce high resolution images of a surface by distinguishing between elastical or inelastical scattering of incident electrons. To do so sample need to be conductive (Colliex 2008). Since the shells were not conductive they were prior to analyzing with SEM mounted onto aluminum stubs using conductive adhesive tape and coated with a gold/palladium layer (Sputter coater SC7640; Quorum Technologies, Lewes, United Kingdom).

3.6 Stable oxygen and carbon isotopes

Before measuring stable isotopes in biogenic calcium carbonate ($CaCO_3$) the carbonate samples needed to be milled from the shell. Three individuals were selected, depending on their age and shell thickness (shell IDs: 01ASGkofj2014, 03ASGkofj2014, 06ASGkofj2014). The $\delta^{18}O$ and $\delta^{13}C$ values of the biogenic shell carbonate were measured using an isotope ratio mass spectrometer (IRMS). Finally they were aligned to calculated $\delta^{18}O$ and $\delta^{13}C$ values of the shell.

3.6.1 Sampling of biogenic calcium carbonate of shells

The sampling of the shell carbonate was carried out with a high precision drill (power pack: Minimo C121; Rotary Handpiece: V11H; Minitor Co., Ltd., Tokyo, Japan) in combination with a binocular microscope (WILD Heerbrugg Gais, Switzerland) and stereo microscope lighting (KL 1500 LCD; Olympus, Hamburg, Germany).

Initially the shells were cross sectioned as described in Section 3.3. Thereafter the epoxy cover was removed using a cylindrical drill bit (Nr. H364E 123 010; Komet/Gebr. Brasseler GmbH & Co. KG, Lemgo, Germany). Additionally leftover parts of the periostracum were removed. In order to maximize the spatial sample resolution, all samples were milled (Dettman and Lohmann 1995) manually.

A cylindrical drill bit (Nr. H364E 123 010; Komet/Gebr. Brasseler GmbH & Co. KG, Lemgo, Germany) was used to mill the $CaCO_3$ samples (Figure 8). As sample region, the increments representing the growth period from 2011 to 2013 including adjacent growth lines were chosen. Sampling was performed in DOG from ontogenetic younger to older shell parts, parallel to the growth lines. The first step was to create an initial-hollow in the ostracum (Figure 8). Shaping the hollow-side, facing sampling direction, parallel to the next growth line is the most important factor. All samples were milled in parallel lines from this side extending the sampling-hollow towards the margin. The extracted carbonate powder was gathered by an underlying weighing paper and successively put into sample-containers. To make sure the sampling follows the growths pattern, adjustments to the hollow-side were made if required. During the sampling procedure the progress was documented in high-resolution copies of the cross section images in order to make the subsequently aligning of the samples more accurate.

Between each sample the drill bit was cleaned by removing left over carbonate with a toothbrush and a paintbrush. Prior to working with a new individual the drill-bit was cleaned by placing it in an ultrasonic bath (Sonorex Super RK510; Bandelin, Berlin, Germany) for 5 min. Cups (1 cm in diameter) held by 4×15 trays with lid, were used as sample-containers (in-house manufacturing, Alfred-Wegener-Institut, Helmholtz-Zentrum für Polar- und Meeresforschung).

Before usage, all cups were first cleaned in an ultrasonic bath for 5 min, followed by rinsing with diluted phosphoric acid.

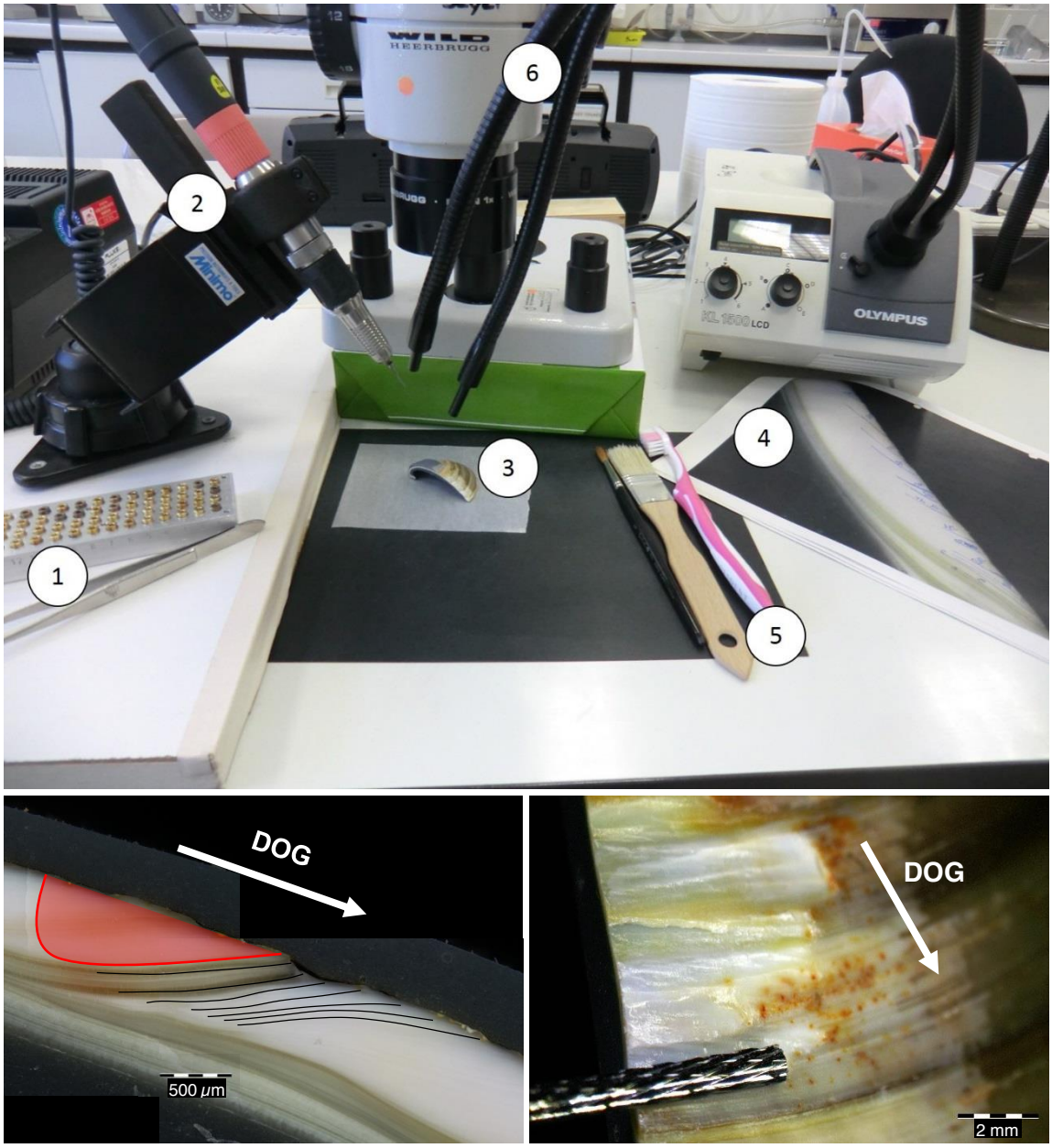

Figure 8: Sampling of calcium carbonate for stable isotopes analysis. Top: General set up. 1 – sample-containers, 2 – high precision drill, 3 – sample on weighing paper, 4 – high-resolution photo of the cross section for documenting the progress, 5 – tools for cleaning the drill bit between each sample, 6 – binocular microscope and lightning system. Bottom-left hand side: Cross section of a shell along the LSG. Red area gives shape of the initial-hollow. Black lines indicate theoretical sampling lines. Resolution not to scale. Bottom-right hand side: Drill bit extending the initial-hollow towards the margin.

3.6.2 Measurement of stable oxygen and carbon isotopes

The ratios of $^{18}O/^{16}O$ and $^{13}C/^{12}C$ were measured using an isotope ratio mass spectrometer (IRMS). This measurement of stable isotopes is based on the fact that charged molecules are deflected differently regarding their weight. This requires the samples to be prior transformed from solid carbonate into CO_2 by dissolving the carbonate samples with phosphoric acid (Budzikiewicz 2005). This was carried out with an automated carbonate preparation device (Kiel IV; Thermo Finnigan, Bremen, Germany). The CO_2 was analyzed in a MAT 253 isotope ratio mass spectrometer (Thermo Finnigan; Bremen, Germany) by ionization and separating according to their mass-to-charge ratio. The measurements were calibrated against to the international NBS-19 standard, reported in δ-notation versus VPDB (Vienna Peedee Belemnite) (Coplen 1994; Craig 1957) and given as parts per million. For $\delta^{18}O$ the long-term precision based on an internal laboratory standard measured over a one-year period was better than ±0.08‰ and better than ±0.06 ‰ for $\delta^{13}C$. For measurement 40 – 100 *µ*g calcium carbonate per sample were weighed in using a precision scales (Sartorius, Göttingen, Germany).

3.6.3 Alignment of measured and calculated $\delta^{18}O$ values

In order to correlate the measured $\delta^{18}O$ of the shell ($\delta^{18}O_{shell}$) with parameters measured from the environment, latter parameters needed to be converted into predicted $^{18}O/^{16}O$ ratios of the shell ($\delta^{18}O_{predicted}$). Afterwards they were assigned chronological in order to align $\delta^{18}O_{shell}$ accordingly.

Calculation of $\delta^{18}O_{predicted}$

The $\delta^{18}O_{predicted}$ values were calculated from ambient sea temperature and salinity measurements (see Section 3.2). First by computing the stable oxygen isotope ratio influenced by salinity ($\delta^{18}O_s$). The calculation was performed using the relationship of salinity of seawater and $\delta^{18}O_s$ described for Kongsfjorden by Maclachlan *et al.* (2007) (Equation 2):

$$\delta^{18}O_s = (0.43 \times S_{sea}) - 14.5 \qquad \textbf{Equation (2)}$$

With: $\delta^{18}O_s$ – Stable oxygen isotope ratio influenced by salinity

S_{sea} – Salinity of the seawater

For further conversion the approach of Grossman and Ku (1986) including a small modification (Dettman *et al.* 1999) was applied (Equation 3). It describes the combined influence of seawater temperature and $\delta^{18}O_s$, on the stable oxygen isotope ratio of biogenetic aragonite. Verification of the crystalline structure of the shell carbonate was carried out using confocal Raman microscopy (CRM, see Section 3.6).

$$\delta^{18}O_{predicted} = (20.6 + 4.34 \times (\delta^{18}O_s - 0.27) - T_{sea}) \times 4.34^{-1}$$

Equation (3)

With:	$\delta^{18}O_{predicted}$	–	Predicted stable oxygen isotope ratio of the shell carbonate
	$\delta^{18}O_s$	–	stable oxygen isotope ratio influenced by salinity
	T_{sea}	–	Temperature of the seawater [°C]

Alignment of $\delta^{18}O_{predicted}$ *and* $\delta^{18}O_{sea}$

An alignment was carried out between the $\delta^{18}O_{predicted}$ and $\delta^{18}O_{sea}$ values. The first step was to arrange the $\delta^{18}O_{predicted}$ values on a time-scale according to their recoding date. Next step was to mark the $\delta^{18}O_{shell}$ values representing the growth line. They were used as an anchor point and aligned first, since it is known that *S. groenlandicus* deposits its growth line in late summer or early fall (Ambrose *et al.* 2012),. Subsequently the data in between were matched point-by-point to the $\delta^{18}O_{predicted}$ graph until the best fit was obtained (Hallmann *et al.* 2008; Versteegh *et al.* 2012).

4 Results

4.1 Representativeness of individual growth

As a sub-population 40 individuals were in 2012 sampled from the enclosure (see Section 3.2). Due to damages to some shells only 27 were suitable for further work. Additionally all ten specimens collected in 2014 were used.

4.1.1 Growth line deposition

A total of 37 individuals were marked with calcein in different years (September) producing 57 possible calcein lines. No animal died during the staining process. Calcein lines were viewed in the cross sections as a thin luminescent line under fluorescent lights (Figure 5). In total all 57 possible calcein marking were verifiable in the shell. Out of 57 possible calcein lines 77 % were visible in the umbo, shell increments showed 91 % (Table 1). The calcein lines were found within the annual growth line, but the position varied. Calcein lines were found at the beginning, in the middle and at the end of growth lines.

Table 1 Verification of the calcein lines, differentiated between umbo and shell.

	2008	2009	2011	Total
Marked	1	33	23	57
Verified:				
Total	1	33	23	57 (100%)
Umbo	1	24	19	44 (77%)
Shell increments	1	28	23	52 (91%)

4.1.2 Growth rate

Figure 9 displays the frequency distribution of increments per year and shell age of the 269 increments measured in 37 shells. The data set covers the time period from 1998 till 2013. Most measurements were possible for the years 2008 – 2011. The oldest individual was 25 years old. The years 1988 – 1997 are represented by less than three increments, respectively. They were excluded from further analysis of the population structure.

The population structure was analyzed by identifying the best fitted (R^2=0.92) von Bertalanffy growth function to represent the shell height-at-age data (Equation 4, Figure 10).

$$SH_t = 69.02 * (1 - e^{-0,15\ (t-1.29)}) \quad \textbf{Equation (4)}$$

With: SH_t – Shell height at time t

t – Time in years

The growth rates of all individuals used for stable isotopes analysis are located within the variability of the population (Figure 10).

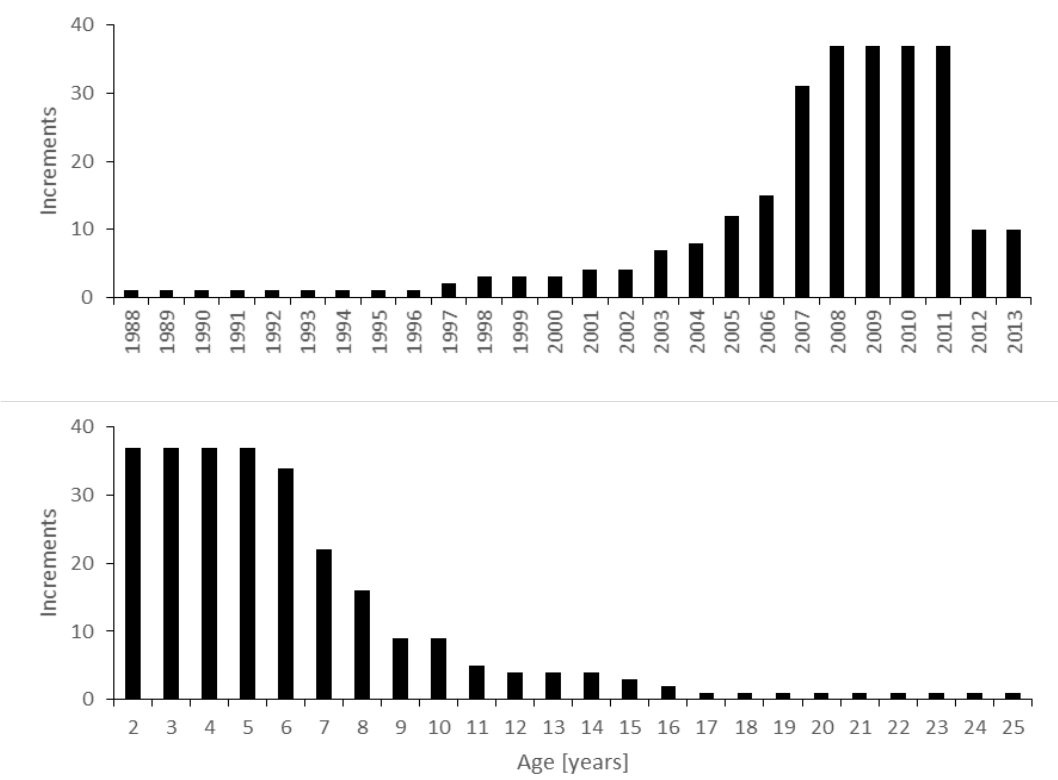

Figure 9: Number of increments per year and ontogenetic shell age. The dataset covered a period of 26 years (1988-2013) while most increments were measured form 2007 to 2011. The oldest specimen became 25 ontogenetic years old.

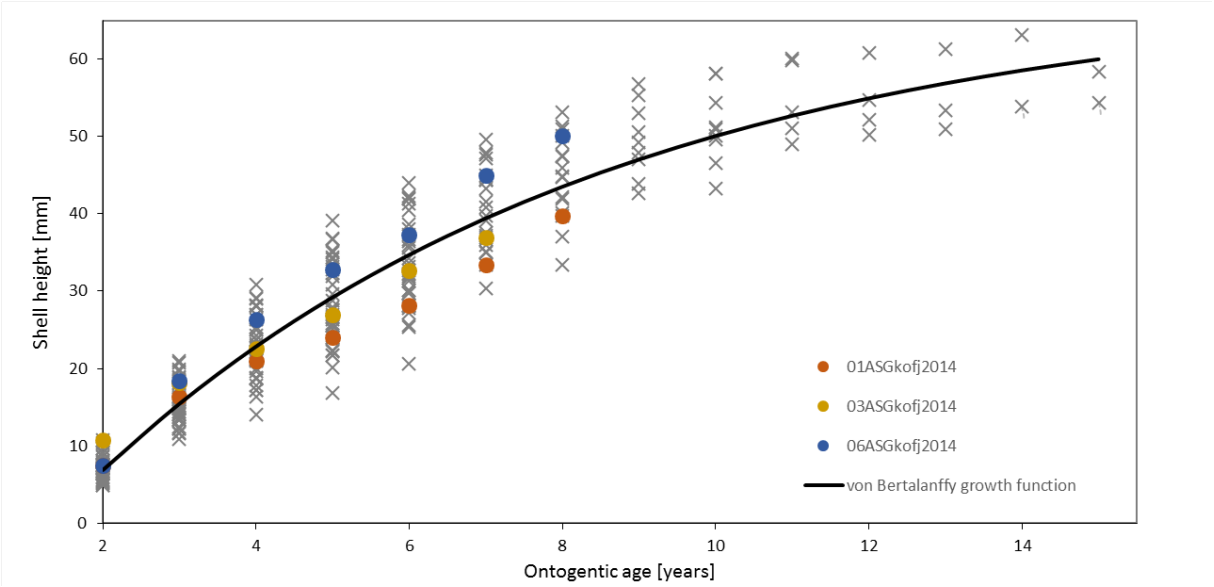

Figure 10: Shell height-at-age data for the shell taken for the *S. groenlandicus* sub-population, including von Bertalanffy growth function with the best fit: $SH_t = 69.02 * (1 - e^{-0{,}15\,(t-1.29)})$. Highlighted are the three shells for stable isotope analysis in red (01ASGkofj2014), yellow (03ASGkofj2014) and blue (06ASGkofj2014). The oldest individual used for the calculation was 15 years.

4.2 Crystalline structure of the shell carbonate

4.2.1 Confocal Raman microscopy

To describe the crystal shell structure, an area within the chosen sample region for the stable isotope analysis was examined (1 μm step width, 0.05 seconds integration time). The spectrum of this area ('sample', Figure 11) was compared to the spectra of an aragonite standard and a calcite standard measured under the same conditions. Figure 11 shows that the sample-spectrum matches the peak positions of aragonite (152 cm^{-1}, 206 cm^{-1}, 705 cm^{-1}, 1085 cm^{-1}; Nehrke and Nouet 2011). A peak at wavenumber 282 cm^{-1}, which is among others identifying for calcite (Nehrke and Nouet 2011) was not detected in the spectrum of the sample.

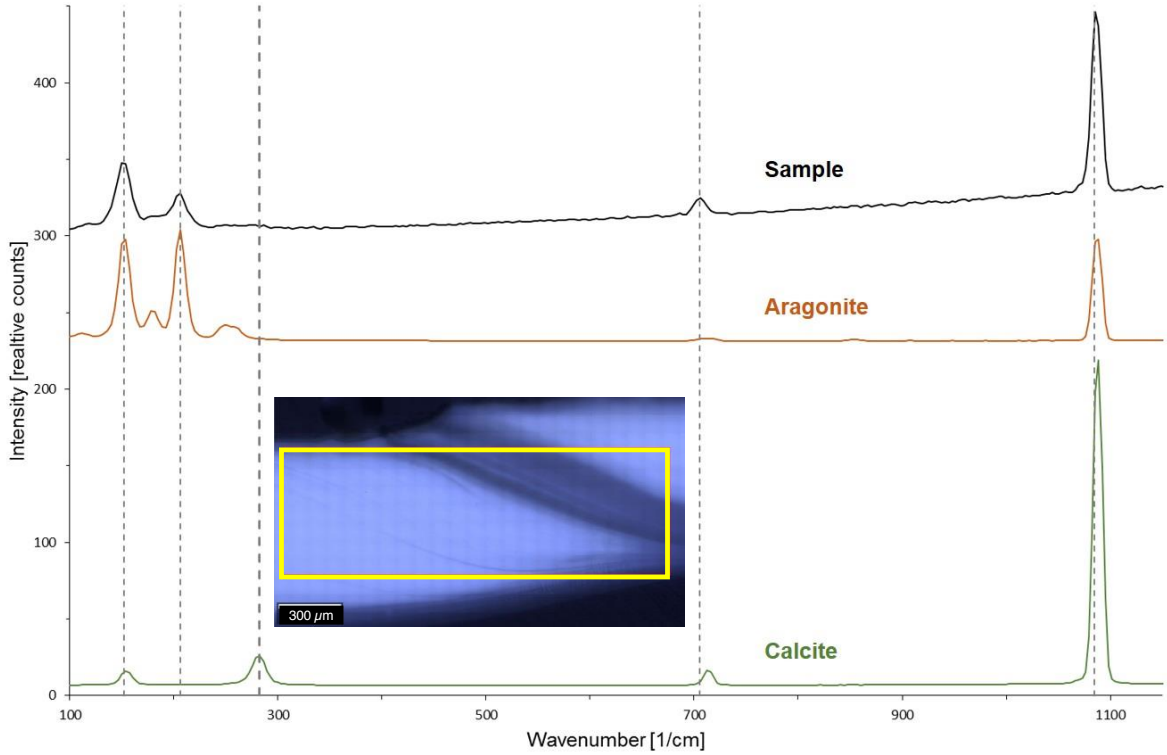

Figure 11: Confocal Raman microscopy map (yellow rectangular shown in inlay image) and spectrum of cross sections of *S. groenlandicus*. Spectra are shown as relative counts (intensity) for each wavenumber in cm^{-1}. The sample spectrum (top black line) matches the most prominent peaks (dotted lines at 152 cm^{-1}, 206 cm^{-1}, 705 cm^{-1} and 1085 cm^{-1}) of the aragonite standard spectrum (middle orange line). It misses the peak of the calcite spectrum (bottom green line) at a wavenumber of 272 cm^{-1}.

The embedding of shells in Araldite caused changes in the outer shell layer. Parts of the shell surface area changed their color. Before embedding in Araldite the surface of effected regions already showed variation in structure. They appeared rougher with higher porosity of the shell. The periostracum was barley present (Figure 12, top). This color variation extended

up to a certain point into the outer shell layer. Those ‘spots’ had sharp contours and occurred along small cracks, following growth lines but mostly as round regions (Figure 12, bottom). Only the ontogenetic younger increments (age 3-4) were affected. Older increments did not show any changes in coloration or structure (Figure 12, middle). The ‘spots’ were also analyzed with CRM. Spectra were measured from a ‘spot’, the nearby unchanged shell and Araldite (Figure 13). The spectrum of the ‘spot’ showed peaks at the determining wavenumbers of aragonite. It also shared peak positions with the spectrum of Araldite. For two shells both variations of one cross section were examined, the cross section with a metal-epoxy coat and after the embedding of this cross section into Araldite. No ‘spots’ were observed in the one without Araldite. There was neither a change in color, nor in the spectrum. However, the regions were ‘spots’ occurred after embedding turned out to have a more reddish color than the rest of the shell. Areas chosen for sampling of calcium carbonate for stable isotopic analysis did not show any ‘spots’.

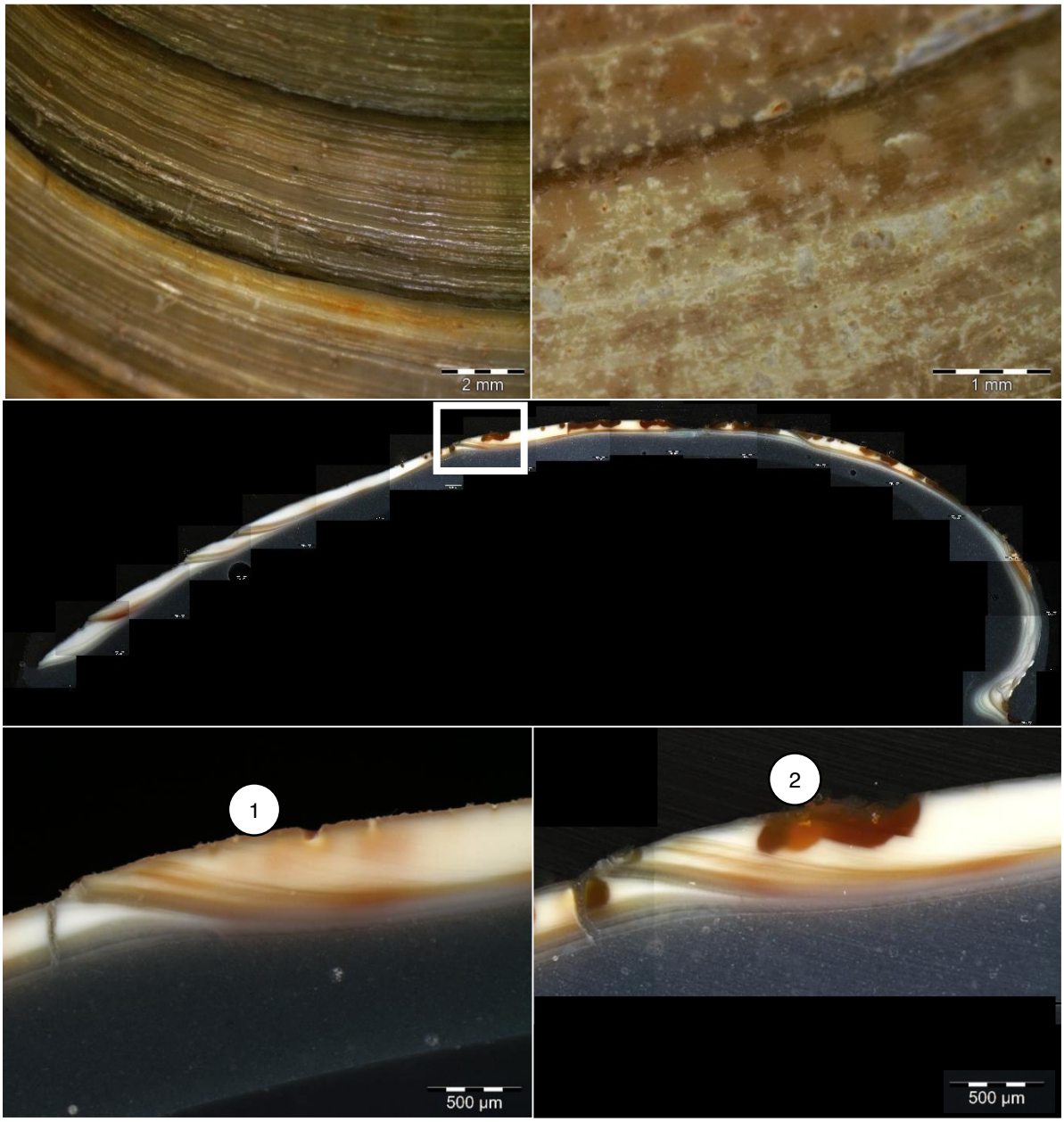

Figure 12: Different images of the shell structure of *S. groenlandicus*. The top two pictures compare the ontogenetic older increments (left) to the ontogenetic younger (right). In ontogenetic younger increments nearly no periostracum was left (dark brown areas). The surface looked damaged. The ontogenetic older part is covered with a periostracum. The middle image shows the distribution of the 'spots'. The last 3-4 increments did not have any 'spots'. The white rectangular is magnified in the bottom two images. Left bottom image is taken before embedding the shell in Araldite. Right bottom image shows the shell cross section after embedding into Araldite. The 'spot' (2) appeared where in the shell cross section had previously a reddish area (1).

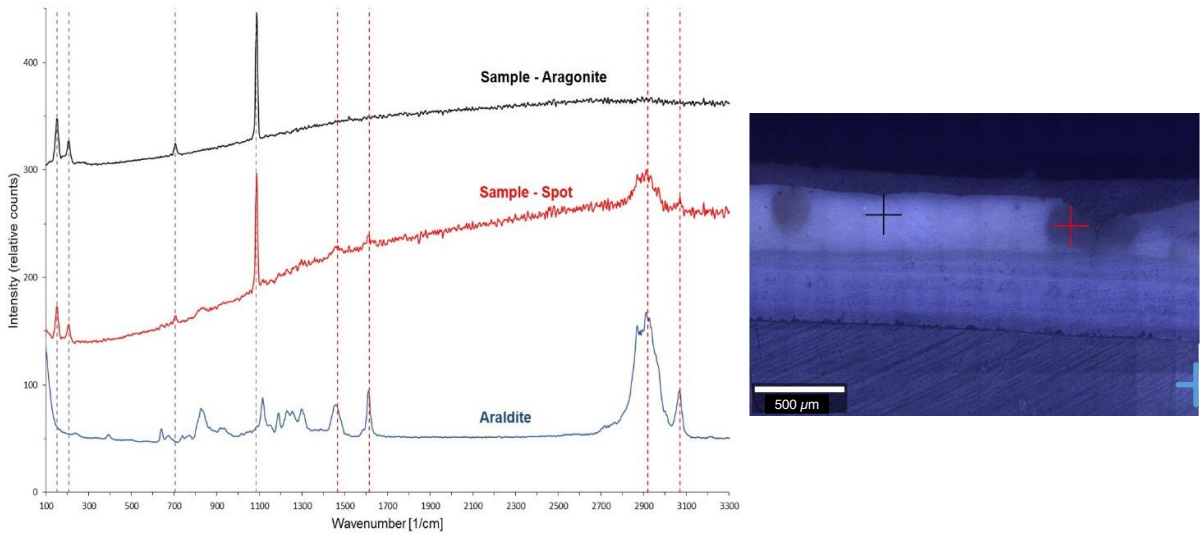

Figure 13: CRM spectra of a region with 'spots'. Colors of the crosses in the shell image match the colors of the spectra. Spectra of the 'spot' (red), an unaffected region (black) and Araldite (blue) are displayed. Black dotted lines indicate the peak positions for aragonite. Red dotted lines point out the peak positions of Araldite.

4.2.2 Electron microscopy

Electron microscopic images were taken from shell cross sections (Figure 14). The cross section of one shell coated with metal-epoxy showed changes in structure in some 'spots' in the outer layer facing the outside. A magnification of the 'spot' area shows a much more porous crystalline structure. After embedding in Araldite those 'spots' did not show the same porous surface. It appeared smoother, but still the structure of the 'spots' differed from the rest of the outer layer as well as from the Araldite.

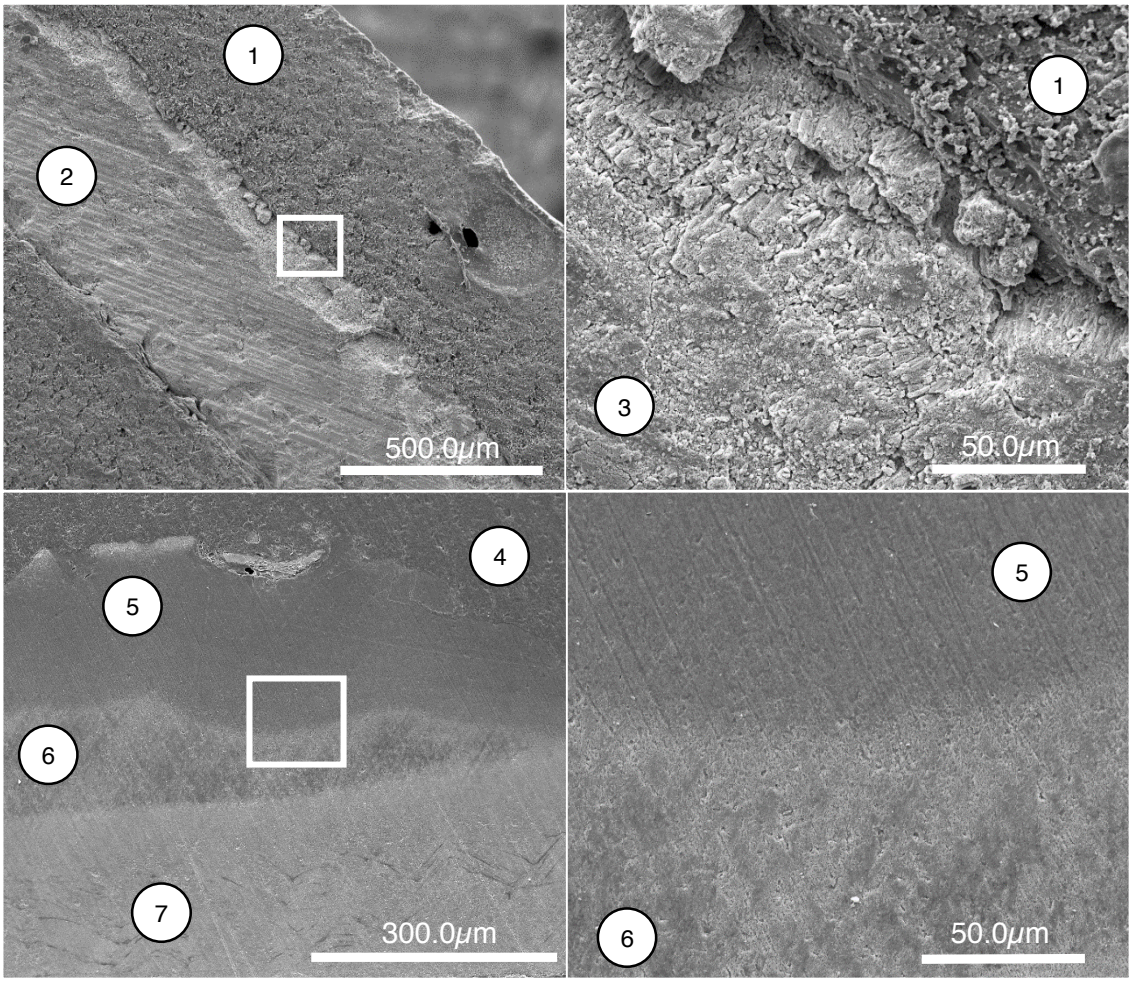

Figure 14: Scanning electron microscope images showing cross sectioned shell of *S. groenlandicus*. Top: Left image is a magnification of the white square shown on the right. The shell (2) is coated with metal-epoxy (1). A change (3) in structure towards the outer side is visible. The magnification shows a porous structure. Bottom: Images of a shell after embedding in Araldite (4). Right image is a magnification of the square outline on the left. The left hand image shows the difference between the inner shell layer (7), outer shell layer (6) and spots (5). Right hand image illustrates the change in spots influenced by Araldite. Differences between (2) and (6), (7) are due to the fact, that the upper shell was not grinded before analysis.

4.3 High resolution sampling of calcium carbonate

Table 2 lists all carbonate samples taken in the shells of three different individuals. Samples were milled manually over a range of three increments, including adjacent growth lines, was sampled subsequently (see Section 3.6.1). Most samples were taken from shell 06ASGkofj2014 (262). A maximum of samples per mm was achieved for 01ASGkofj2014 (15.4). Average sampling intervals were 0.065 mm (01ASGkofj2014), 0.074 mm (03ASGkofj2014) and 0.066 mm (06ASGkofj2014).

Table 2 *S. groenlandicus*: List of carbonate samples taken from three shells (01ASGkofj2014, 03ASGkofj2014 and 06ASGkofj2014). Numbers of carbonate samples in total for each shell, as well as differentiated by lighter and darker increments.

	01ASGkofi2014	03ASGkofi2014	06ASGkofi2014
Total sample number	242	196	262
Samples taken in lighter increment	165	138	182
Samples taken in darker increment	77	58	80
Total width of sampling range [mm]	15.8	14.5	17.3
Resolution [samples×mm^{-1}]	15.4	13.6	15.2

4.4 Stable oxygen and carbon isotopes

Calcium carbonate samples were taken from three individuals (shells IDs: 01-, 03-, 06ASGkofj2014). The samples taken within each shell were distributed over the increments approximately covering the period from winter 2010 to winter 2013. The ontogenetic age of the increments was 6 – 8 years (01-, 06ASGkofj2014) and 5 – 7 years (03ASGkofj2014), respectively. In total 392 samples were measured. Most measurements were carried out with carbonate samples from 03ASGkofj2014 (178 measurements) followed by 108 measurements from 01ASGkofj2014 and 106 measurements from 06ASGkofj2014. All $\delta^{18}O_{shell}$ values are displayed in Figure 15 in DOG with equal spacing. The amplitude of all values was 3.53 ‰. Shell 01ASGkofj2014 had a range of 2.61 ‰ (1.46 – 4.07 ‰). Shells 03ASGkofj2014 and

06ASGkofj2014 had a range of 2.75 ‰ (1.19 – 3.94 ‰) and 1.82 ‰ (2.01 – 3.90 ‰), respectively. The samples covered approximately three growth periods and additionally one ending of a growth period at the beginning of sampling. A new growth period starts with the maximum value recoded after a growth line. After this peak values gradually decrease to a minimum and before increasing sharply. The saw-toothed shape is noticeable in all three profiles (Figure 15).

Figure 16 shows the measured temperature, salinity values and the calculated $\delta^{18}O_{predicted}$ values. The data cover the period from January 2010 to September 2014. Due to technical malfunction data are missing from June 2011 to September 2012. Time intervals between measurements were 10 minutes. A maximum temperature of 7.00 °C and a minimum of -2.05°C was recorded. The salinity ranged from 19.33 to 32.72. Thus the $\delta^{18}O_{predicted}$ values had a maximum of 4.11 ‰ and a minimum of -3.11 ‰ (calculation see 3.6.3). Temperature and salinity profiles showed inverse maximum and minimum occurrence with maximum temperature and minimum salinity from May to August (Figure 16).

The $\delta^{18}O_{shell}$ values were aligned to the $\delta^{18}O_{predicted}$ values (Figure 17). Since $\delta^{18}O_{predicted}$ data are missing from June 2011 to September 2012 the $\delta^{18}O_{shell}$ values approximately representing this period of time, were plotted roughly according to aligned $\delta^{18}O_{shell}$ values in order of sampling. Since growth line deposition occurs around September $\delta^{18}O_{shel}$ values measured in growth lines were roughly anchored in late summer Section 4.1.1). Nevertheless, it is noted, that the course over the whole period of time for all shells is very similar in their decline, increase, maxima and minima values. They showed the same sample density pattern with most samples aligned from February to August in each year. Growth line samples have been aligned more widely spaced. The first peak $\delta^{18}O_{shell}$ values of all shells in DOG of is higher than the maximum values of $\delta^{18}O_{predicted}$. The third peak was aligned more accurately since in all data sets the values are similar. In the first growth line the $\delta^{18}O_{shell}$ values did not get as low as the $\delta^{18}O_{predicted}$ values. For the other growth lines it is not possible to see if the $\delta^{18}O_{shell}$ value recoded the minimum in $\delta^{18}O_{predicted}$ since the calculated data are unavailable or partly missing for this period of time. In general the aligned $\delta^{18}O_{shell}$ data showed a similar course as the predicted values.

The $\delta^{13}C$ values are presented in Figure 18. They were aligned according to the $\delta^{18}O_{shell}$ values. The largest range was 3.30 ‰ measured in 03ASGkofj2014 followed by 1.7 ‰ for 01ASGkofj2014 and 1.46 ‰ for 06ASGkofj2014. Thus, 03ASGkofj2014 was most variable, especially between growth lines and the rest of the increment. 06ASGkofj2014 was least variable throughout the measured years. Furthermore, 06ASGkofj2014 values of the first, second and last growth line tend to be more negative. In comparison the third growth line

showed the least variation. In general was the variability of $\delta^{13}C$ values among the specimens higher the one observed for $\delta^{18}O_{shell}$ values.

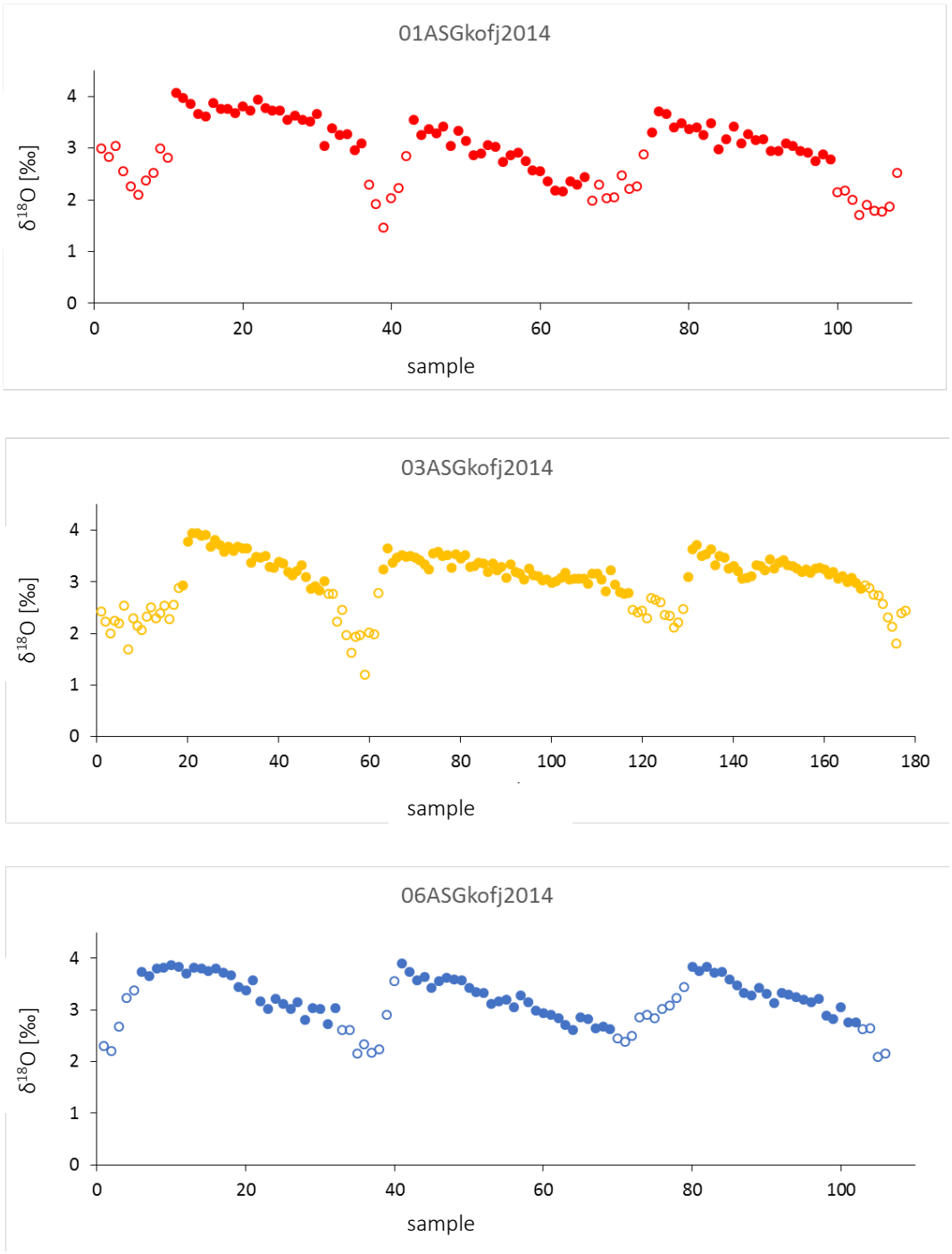

Figure 15: $\delta^{18}O$ values for all three individuals displayed with equal spacing. Empty circles represent the samples taken in a growth line. All three profiles showed minimum values in growth lines followed by a sharp increase and a gradual decrease. Each profile started with the end of a growth period (ending with the first minimum) and three approximately complete growth cycles (from peak after a growth line until ending of the next growth line).

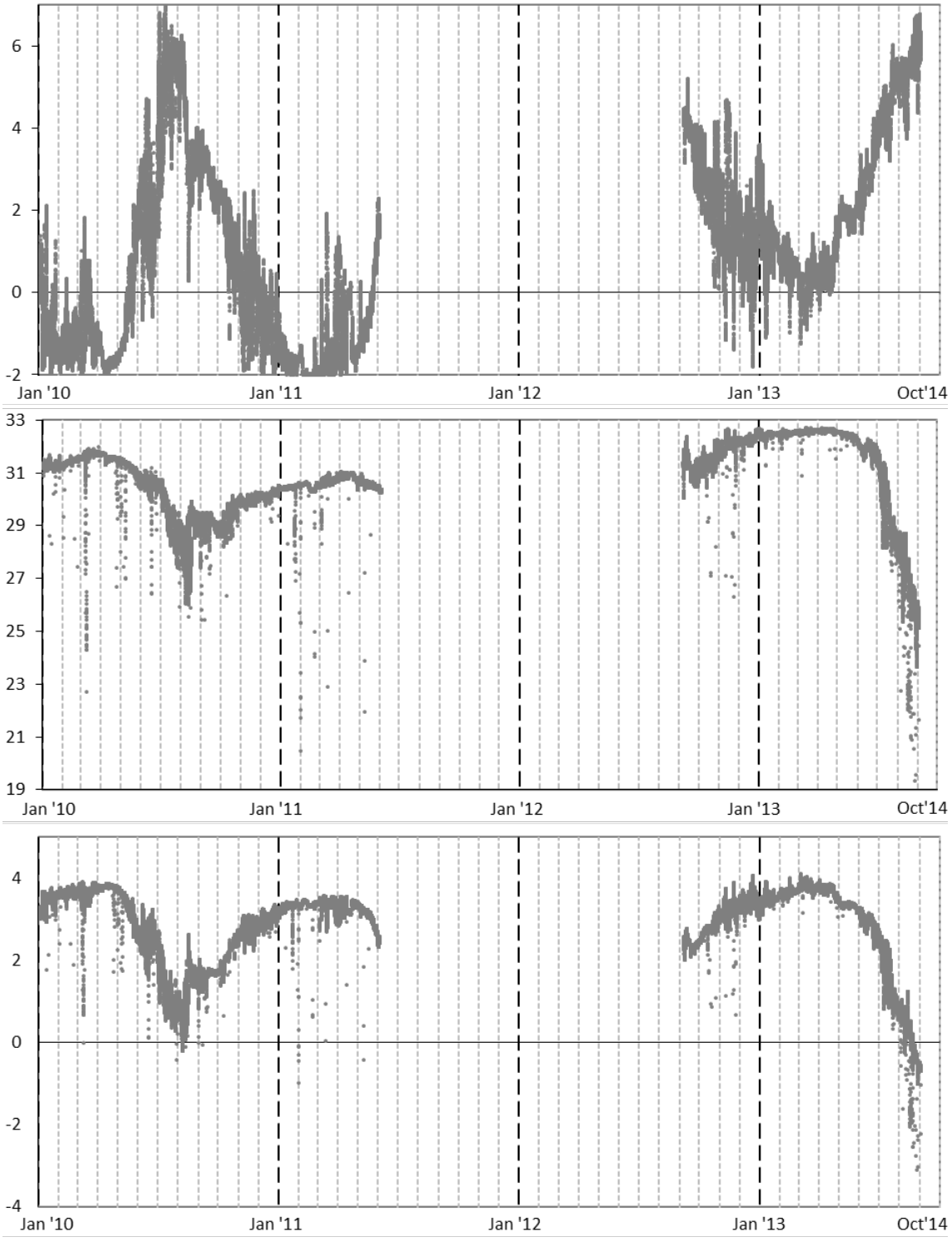

Figure 16: Seawater temperature, salinity and $\delta^{18}O$predicted at the study site. Temperature and salinity were measured. $\delta^{18}O_{predicted}$ has been calculated from these measured in situ values. The vertical dotted lines indicate the first day of each month. The profiles covered the time period from January 2010 until September 2013 (missing data from June 2011 until September 2012 due to malfunction of the instrument). The temperature profile is invers to the profiles of salinity and $\delta^{18}O_{predicted}$. Maximum temperature and minimum salinity/$\delta^{18}O_{predicted}$ values were reached in from May until August.

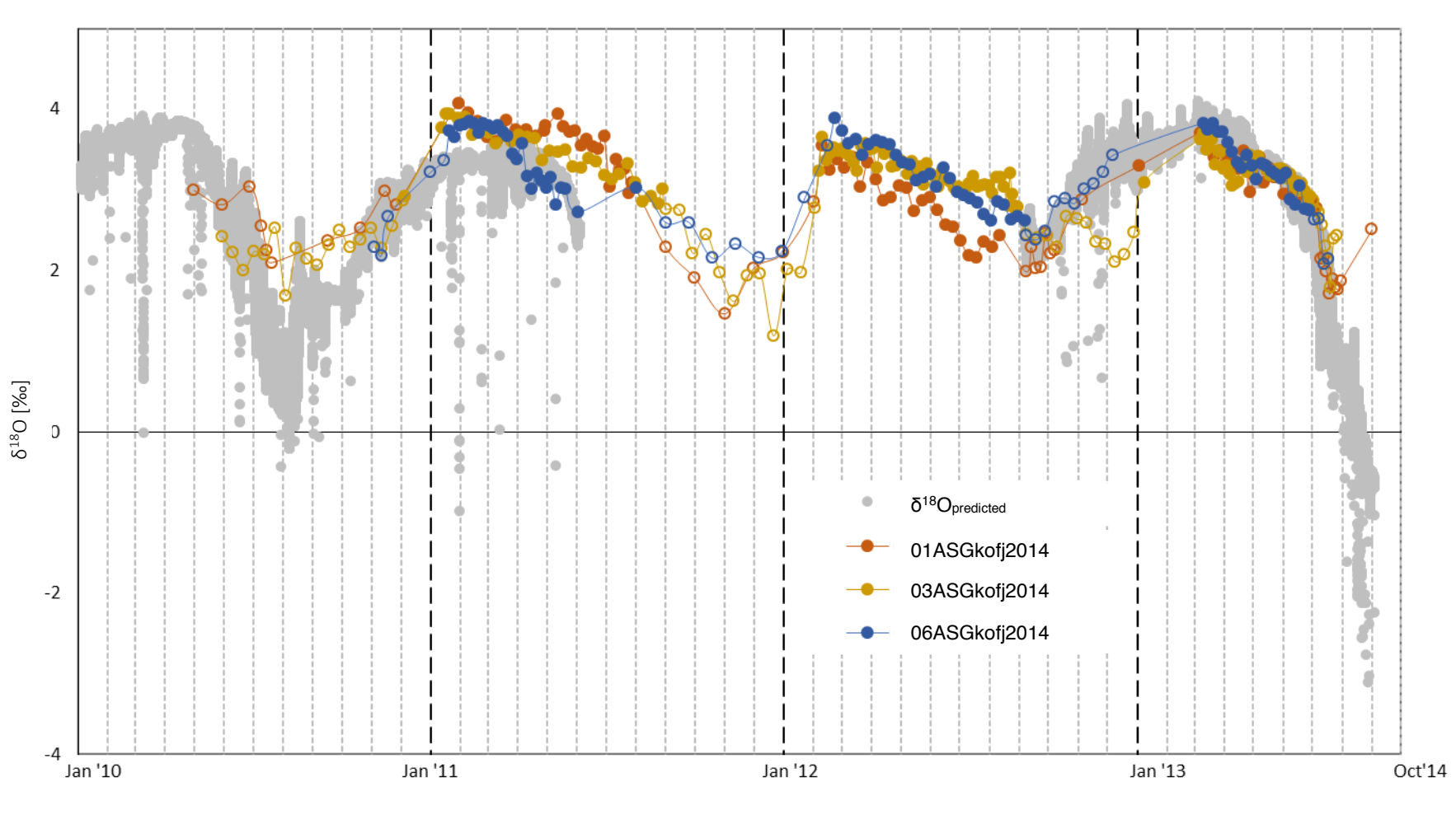

Figure 17: Alignment of $\delta^{18}O_{shell}$ and $\delta^{18}O_{predicted}$ values. Included are all values measured in *S. groenlandicus* shells 01ASGkofj2014 (red), 03ASGkofj2014 (yellow) and 06ASGkofj2014 (blue). They were manually aligned with the $\delta^{18}O_{predicted}$ (gray). Dotted lines mark the first day of each month. The seasonal pattern between measured and predicted data is very similar. Additionally the $\delta^{18}O_{shell}$ values did not show big differences among the shell. Empty circles are measurements of carbonate samples taken within growth lines.

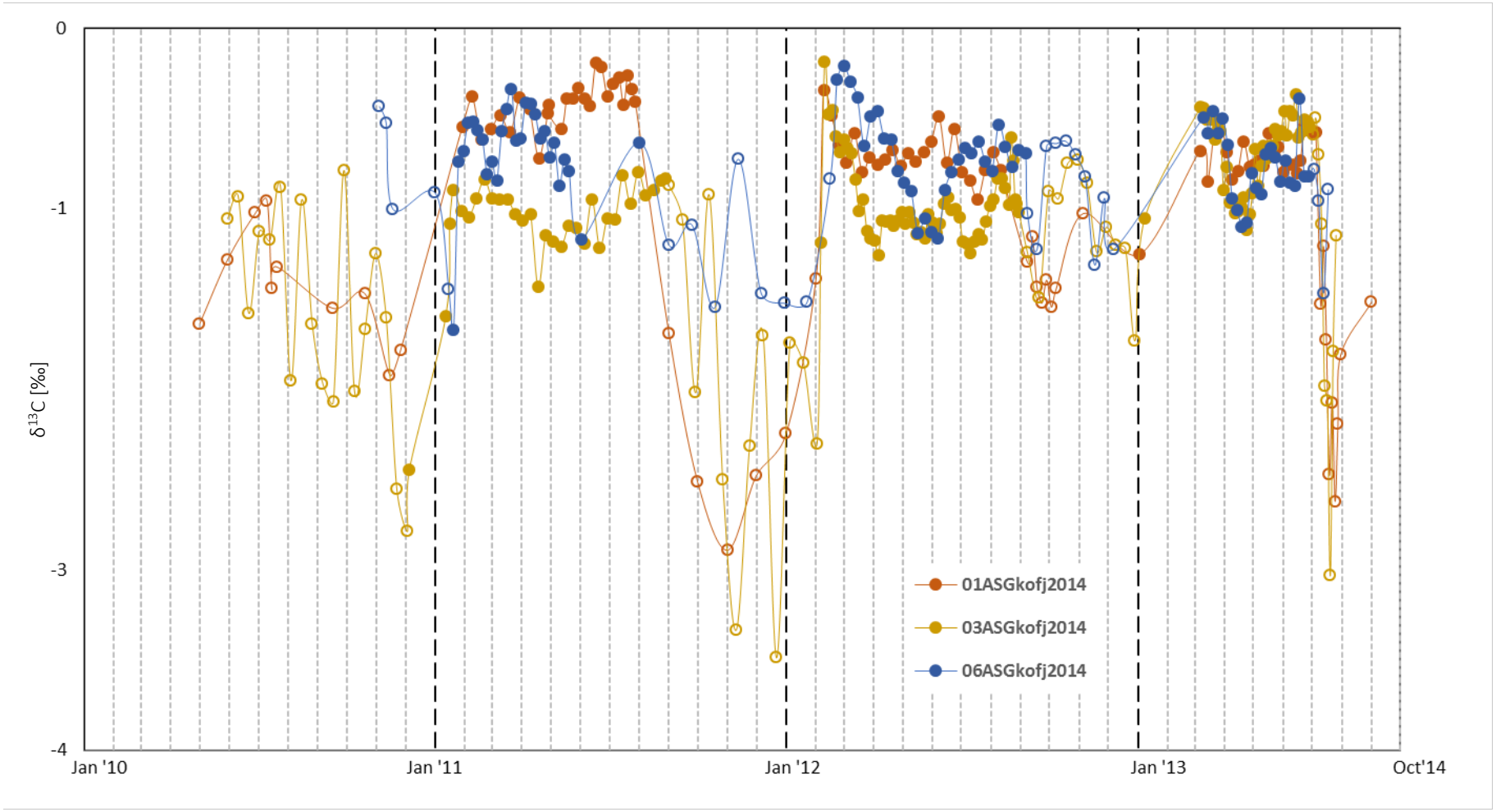

Figure 18: $\delta^{13}C$ values of shell carbonate taken from *S. groenlandicus* shells 01ASGkofj2014 (red), 03ASGkofj2014 (yellow), and 06ASGkofj2014 (blue). Arrangement according to the aligned $\delta^{18}O_{shell}$ values (see Figure 17). Empty circles represent samples taken from growth lines. Vertical dotted lines represent the first day of each month. Values show maximum variability in the first, second and fourth growth line.

5 Discussion

5.1 Representativeness of individual growth

Measuring the increments of the entire sub population of Greenland cockles was done to show, that the three individuals, which were chosen for stable isotope analysis, are representative regarding their general shell growth. Their shell height-to-age ratios all were situated within the one of the sub-population and therefore they were concluded to be representative individuals. The scatter resemble those published by Kilada *et al*. (2007) for *S. groenlandicus*. It is not possible to compare the calculated values of the von Bertalanffy equation because the maximum age of 15 is much younger than the specimens used by for instance Carroll *et al*. (2011) or Ambrose *et al*. (2006).

However, the timing of deposition of growth lines agrees approximately with the findings of Ambrose *et al*. (2006). They found that all examined cockles already started the formation of a growth line at the time of marking (August) with calcein. They too noted that the position of the calcein within the growth line differs between individuals. The growth lines examined in this study were all in formation at the time of marking (September). In some shells the calcein line was located at the very beginning of the growth line, indicating, that the formation had just started. Ambrose *et al*. (2006) suggest that the formation of the growth line is more likely triggered by food availability than by seawater temperature.

In general shell growth may been influenced by environment changes related to shell capture and relocating them into the enclosure. Further, the enclosure e.g. disables the proper removal of drifting macroalgae. This may have caused changes in the immediate surroundings of single individuals. However, the setup of collecting individuals into an enclosure on the sea floor is believed to be much more equal to the natural habitat of the cockles than holding them in baskets above the sea floor without any sediment (Ambrose *et al*. 2012).

5.2 Crystalline structure of the shell carbonate

The matching peak positions between the spectrum of the shell carbonate and the aragonite standard spectrum (Figure 11) demonstrate that the shells of *S. groenlandicus* are aragonitc. This matches with the findings of Khim *et al*. (2003) who examined carbonate powder with X-ray diffraction analysis. An aragontic crystalline structure commonly observed in bivalves species (e.g. Bušelić *et al*. 2014; Gillikin *et al*. 2007; Schöne 2013), other than the ‘spots’ that occurred after embedding shells in Araldite (Figure 12). The SEM images showed that there are areas, which are much more porous than the rest of the shell (Figure 12). This may be due to the missing periostracum on the surface of the affected increments. Without the

protection of this conchiolin layer the shell carbonate is directly exposed to environmental conditions such as pH of the seawater, mechanical abrasion caused by sediment or biological influences. If this is the case it is most likely that fossil shells of *S. groenlandicus* have even larger areas with this variation.

Still the structure is uncommon, since the Araldite intruded the carbonate (matching peak positions in Figure 13). An intrusion of Araldite is desired when it comes to really fragile structures such as some coral skeletons. Here Araldite is used to fill porous structures in order to stabilize them for further treatment. However, the embedding is carried out under vacuum to achieve an intrusion of the Araldite (Carreiro-Silva *et al.* 2005; Chazottes *et al*. 2009). In case of *S. groenlandicus* no vacuum is necessary for that.

Nevertheless, the potential of *S. groenlandicus* to function as a climate archive is most likely not influenced by this variation in the shell carbonate. This is because in shells examined prior to embedding no variation in the Raman spectrum was found whereas afterwards 'spots' were visible and detectable (Section 4.2.1). But it is necessary to confirm this by measuring $\delta^{18}O_{shell}$ values taken from areas indicating those 'spots'.

5.3 High resolution sampling for calcium carbonate

It was strived for a high resolution of carbonate samples. Therefore the approach of milling carbonate (Dettman and Lohmann 1995) manually was applied. The achieved resolution in the present study by manually milling (65 μm) is nearly ten times higher than the resolution reached by drilling calcium carbonate (< 500 μm) (Khim 2002). By using a computer-controlled micropositioning technology for milling $CaCO_3$ samples from the shell Dettman and Lohmann (1995) achieve a resolution of 20 μm. This resolution is three times higher than the minimum average of 65 μm presented in this study. However, this is due to the differences in minimum sample sizes for IRMS analysis. Dettman and Lohmann (1995) sampled approximately 10 μg of carbonate, in contrast the range of measurable sample masses for this study was 40 – 100 μg. Thus, the carbonate sample weights of *S. groenlandicus* needed to be two to five times bigger. In general a greater sample number would have been possible, if the minimum sample size for mass spectrometry were smaller. Therefore the resolution of samples is rather a question of minimum sample mass than of the ability to mill minimum sections from the shell. Hence under the given circumstances the obtained samples number per micrometer is considered to be high.

A difficulty during sampling was the variation in hardness of the carbonate, not only between lighter and darker increments but also within them. Where these hard zones occurred it was difficult to obtain the parallelism between sampling lines. It also increased the risk of the drill bit slipping over the edge of the hollow contaminating the sample leading to discard of

samples. Contrary to the expectations of the shell being fragile and thin this was no problem. None of the sampled shell broke during handling.

5.4 Stable oxygen and carbon isotopes

The aim of this study was to calibrate high resolution $\delta^{18}O$ values measured in shell carbonate of *S. groenlandicus* predicted $\delta^{18}O$ shell values of the ambient water. Therefore 392 $\delta^{18}O$ values were subsequently measured in shell carbonate of three individuals. The $\delta^{18}O$ values of all shells showed the same seasonal periodicity with lower $\delta^{18}O$ values in the growth line (Figure 15) as already reported by Khim (2002) and Khim *et al.* (2003). They concluded, that *S. groenlandicus* records seasonal cycles of salinity and temperature fluctuations. The presented study went one step further by directly comparing the $\delta^{18}O_{shell}$ values with predicted $\delta^{18}O$ values specific to the sampling site and time of the examined cockles.

It was possible to align at least two maximum and two minimum peaks of the $\delta^{18}O_{shell}$ values to peaks in $\delta^{18}O_{predicted}$ values. Where the implementation was possible the alignment between the measured and calculated $\delta^{18}O$ values (Figure 17) suggest a strong similarity. The pattern of a seasonal cyclicity became obvious even though none of the shell actually recorded the most negative $\delta^{18}O_{predicted}$ values. This indicated that the growth of *S. groenlandicus* was limited by either the maximum of temperature or the minimum of salinity. Both events occur at the same time of the year and lead to those minimum of $\delta^{18}O_{predicted}$ not reported by the shell. Despite that, two out of three maxima in $\delta^{18}O_{shell}$ matched to the comparison $\delta^{18}O_{predicted}$ values. There was a distinctive higher density of samples at the beginning of each growth period (Figure 17). Consequently, it is assumed, that growth rate was much higher from March to July, especially compared to the widely spaced values of the growth line aligned in August – February. Thus the time of maximum growth is roughly the same also presented in Kilada *et al*. (2007). All three shells examined here showed lowest $\delta^{18}O$ values during time of growth line deposition, which means in July – October, when water temperature was. This supports the findings of Section 5.1.1 that the growth line is deposited annually in late summer to early fall.

A misalignment occurred at the beginning of 2011. Here the $\delta^{18}O_{shell}$ values are higher than the $\delta^{18}O_{predicted}$ values. This may be due to a change in the shell carbonate composition or an incorrect measurement of temperature and salinity. Since the offset is more or less identical in all shells and $\delta^{18}O_{shell}$ values reached very similar values in all measured years the latter is assumed to be more likely. Due to spatial differences between the shells enclosure and the data logger an offset might (to a minor degree) be explained by different environment parameters surrounding them. Additionally, drifting macroalgae caught in the enclosure could have had an influence on the cockles. Due to the lacking comparison data it is not possible to

check the further course for this offset. In December 2012 the shell 03ASGkofj2014 had values represent six outliers. Since the other shells did not show similar values this is considered to be individual to the shell.

However, these findings need to be interpreted with caution since neither the comparison data, nor the $\delta^{18}O_{shell}$ data set is complete nor sufficient. The alignment of the $\delta^{18}O_{shell}$ values is based on subjective assessment. What could make this less inaccurate would be to measure $\delta^{18}O_{shell}$ values over a longer period of time in order not to sample unfinished growth cycles and to have continuously measured temperature and salinity data. Calcein markings within the sample region would have been of use as an anchor points for the alignment. Additionally, it need to be considered, that $\delta^{18}O_{shell}$ values are influenced by temperature as well as salinity. Calculations using mean values for e.g. salinity is difficult since the salinity fluctuation in Kongsfjorden is high (Figure 16). $\delta^{13}C$ values of the shells carbonate tended to be vary between individuals (Figure 18). Specimen 03ASGkofj2014 showed periodically alterations between more negative $\delta^{13}C$ values during growth line depositions (late summer) compared to the rest of the year. Whereas 06ASGkofj2014 did not show such a pattern. The third growth line however does not show any periodicity. None of the shells decreased in $\delta^{13}C$ values at that time. Khim *et al.* (2003) found periodically cycles in $\delta^{13}C$ values for *S. groenlandicus* with minima in growth lines as observed in the shells 01- and 03ASGkofj2014. They assume that it is either due to an increase in particular organic matter (POM) caused by an estuary influx or a ^{12}C-enriched CO_2 release caused by remineralization of POM, since there is no evidence for a phytoplankton bloom in summer. However, Ambrose *et al.* (2012) present fluorescence data as an indicator for phytoplankton blooms with a peak in June for Kongsfjorden. These blooms influence the dissolved inorganic carbon after remineralization and therefor the $\delta^{13}C$ of shell carbonate. In Kongsfjorden an influence of meltwater inflow is also possible (Svendsen *et al.* 2002). Regarding the third sampled growth line it might be possible, that the prior influence on the $\delta^{13}C$ lagged in that year. However, none of that explains the big differences between the shells 01-, 03ASGkofj2014 and the shell 06ASGkofj2014 since it is hardly explainable to have such environmental differences within a 3 × 3 m area (area of enclosure). Hence there must be another reason for the variation of $\delta^{13}C$ values in *S. groenlandicus*, which is not understood yet.

6 Conclusion and outlook

This study is the first to successfully calibrate high resolution $\delta^{18}O$ values measured in the aragonitic shell carbonate of *S. groenlandicus* against predicted $\delta^{18}O$ shell values, calculated from temperature and salinity measurements. The calibrated data show strong similarity between the shell and predicted $\delta^{18}O$ values as well as among the shells. It is concluded that $\delta^{18}O$ values within the shells of *S. groenlandicus* are incorporated in equilibrium with the $\delta^{18}O$ composition of the ambient seawater, only influenced by temperature and salinity. Nevertheless, further validation of the findings is considered necessary, i.e. covering a longer period of time as well as analyzing more individuals in the *in situ* setup at Kongsfjorden. It is also recommended to use additional calcein markings within the sample area of calcium carbonate for a more accurate alignment. In order to cover a longer period of time within one shell it is necessary to clarify why the shells showed porous 'spots' in the ontogenetic younger increments and if they influence the stable isotope ratios. Furthermore it was noted that the reconstruction of seawater temperature or salinity is challenging since the $\delta^{18}O_{shell}$ ratios are influenced by these two environmental parameters, affecting processes of biomineralization. This is a common issue when using proxies, which are influenced by more than one environmental parameter. One possible future solution for the development of a solely temperature dependent proxy in *S. groenlandicus* the analysis of clumped isotopes in the shell carbonate (Ghosh *et al.* 2006). Unlike the analysis of stable isotope ratios this method analyses the distribution of specific isotopologues (Ghosh *et al.* 2006). The advantage of this approach is that it only depends on temperature, which makes it possible to reconstruct temperature without assuming salinity values. However, this would first require a habitat and species-specific calibration similar to this study.

7 References

Ambrose, Jr. W. G., Renaud, P. E., Locke V, W. L., Cottier, F. R., Berge, J., Carroll, M. L., Levin, B., Ryan, S. 2012. Growth line deposition and variability in growth of two circumpolar bivalves (*Serripes groenlandicus*, and *Clinocardium ciliatum*). Polar Biology 35:345–54.

Ambrose, Jr. W. G., Carroll, M. L., Greenacre, M., Thorrold, S. R., McMahon, K. W. 2006. Variation in *Serripes groenlandicus* (Bivalvia) Growth in a Norwegian high-Arctic fjord: Evidence for local- and large-scale climatic forcing. Global Change Biology 12:1595–1607.

Baross, J. A., Hoffman, S. E. 1985. Submarine hydrothermal vents and associated gradient environments as sites for the origin and evolution of life. Origins of Life 15(4):327–45.

Budzikiewicz, H.. 2005. Massenspektrometrie: Eine Einführung. 5th Edition. Weinheim: Wiley-VCH Verlag GmbH & Co.

Bušelić, I., Peharda, M., Reynolds, D. J., Butler, P G., González, A. R., Ezgeta-Balić, D., Vilibić, I., Grbec, B., Hollyman, P., Richardson, C. A. 2014. *Glycymeris bimaculata* (Poli, 1795) - A New sclerochronological archive for the Mediterranean? Journal of Sea Research 95:139–48.

Carreiro-Silva, M., McClanahan, T. R., Kiene, W. E. 2005. The role of inorganic nutrients and herbivory in controlling microbioerosion of carbonate substratum. Coral Reefs 24:214–21.

Carroll, M. L., Ambrose, Jr. W. G., Levin, B. S., Locke, V,. William L., Henkes, G. A., Hop, H., Renaud, P. E. 2011. Pan-Svalbard growth rate variability and environmental regulation in the Arctic bivalve *Serripes groenlandicus*. Journal of Marine Systems 88:239–51.

Catling, D. C., and Claire, Mark. W. 2005. How Earth's atmosphere evolved to an oxic state: A status report. Earth and Planetary Science Letters 237:1–20.

Chazottes, V., Cabioch, G., Golubic, S., Radtke, G. 2009. Bathymetric zonation of modern microborers in dead coral substrates from New Caledonia-Implications for paleodepth reconstructions in holocene corals. Palaeogeography, Palaeoclimatology, Palaeoecology 280:456–68.

Colliex, C. 2008. Elektronenmikroskopie: Eine anwendungsbezogene Einführung. 1st Edition. Stuttgart: Wissenschaftliche Verlagsgesellschaft.

Coplen, T. B. 1994. Reference and intercomparison materials for stable isotopes of light elements. Pure & Appl. Chem 273–276.

Cottier, F., Tverberg, V., Inall, M., Svendsen, H., Nilsen, F., Griffiths, C. 2005. Water mass modification in an Arctic fjord through cross-shelf exchange: The seasonal hydrography of Kongsfjorden, Svalbard. Journal of Geophysical Research 110: Issue 12: 1–18.

Craig, H. 1957. Isotopic standards for carbon and oxygen and correction factors for mass-spectrometric analysis of carbon dioxide. Geochimica et Cosmochimica Acta 12:133–49.

Dettman, D. L., Lohmann, K. 1995. Microsampling carbonates for stable isotope and minor element analysis: Physical separation of samples on a 20 micrometer scale. Journal of Sedimentary Research 65:566–69.

Dettman, D. L., Reische, A., Lohmann, K. 1999. Controls on the stable isotope composition of seasonal growth bands in aragonitic fresh-water bivalves (Unionidae). Geochimica et Cosmochimica Acta 63(7/8):1049–57.

Elverhdi, A., Lonne, O., Seland, R. 1983. Glaciomarine sedimentation in a Modern fjord environment, Spitsbergen. Polar Research (1):127–49.

Epstein, S., Buchsbaum, R., Lowenstam, H., Urey, H. C. 1961. Carbonate-water isotopic temperature scale. Bulletin of the Geological Society of America 62:417–26.

Epstein, S,, Mayeda, T. 1953. Variation of 18O content of water from natural sources. Geochimica et Cosmochimica Acta 4:213–24.

Fischer, G., Wefer, G. 1999. Use of proxies in paleo-oceanography: Examples from the South Atlantic. Berlin, Heidelberg: (c) Springer-Verlag.

Gosh, P., Adkins, J., Affek, H., Balta, B., Guo, W., Schauble, E. A., Schrag, D., Eiler, J. M. 2006. 13C-18O bonds in carbonate minerals: A new Kind of paleo-thermometer. Geochimica et Cosmochimica Acta 70:1439–56.

Gillikin, P. D., Lorrain, A., Meng, L., Dehairs, F. 2007. A large metabolic carbon contribution to the δ13C record in marine aragonitic bivalve shells. Geochimica et Cosmochimica Acta 71:2936–46.

Grossman, E. L., Ku, T. 1986. Oxygen and carbon isotope fractionation in biogenic aragonite: Temperature effects. Chemical Geology 59:59–74.

Hallmann, N., Burchell, M., Schöne, B. R., Irvine, G. V., Maxwell, D. 2009. High-resolution sclerochronological analysis of the bivalve mollusk *Saxidomus gigantea* from Alaska and British Columbia : Techniques for eevealing Environmental archives and archaeological seasonality. Journal of Archaeological Science journal 36:2353–64.

Hallmann, N., Burchell, M., Schöne, B. R., Strom, A., Fiebig, J. 2008. An intractable climate archive — sclerochronological and shell oxygen isotope analyses of the Pacific geoduck *Panopea abrupta* (bivalve mollusk) from Protection Island (Washington State, USA). Palaeogeography, Palaeoclimatology, Palaeoecology 269:115–26.

Herrmann, M., Lepore, M. L., Laudien, J., Arntz, W. E., Penchaszadeh, P. E. 2009. Growth estimations of the Argentinean wedge clam *Donax hanleyanus*: A comparison between length-frequency distribution and size-increment analysis. Journal of Experimental Marine Biology and Ecology 379:8–15.

Hop, H., Pearson, T., Hegseth, E. N., Kovacs, K. M., Wiencke, C., Kwasniewski, S., Eiane, K., Mehlum, F., Gulliksen, B., Wlodarska-Kowalczuk, M., Lydersen, C., Weslawski, J. M., Cochrane, S., Gabrielsen, G. W., Leakey, R. J. G., Lønne, O. J., Zajaczkowski, M., Falk-Petersen, S., Kendall, M., Wängberg, S. A., Bischof, K., Voronkov, A. Y., Kovaltchouk, N. A., Wiktor, J., Poltermann, M., Prisco, G., Papucci, C., Gerland, S. 2002. The marine ecosystem of Kongsfiorden, Svalbard. 21(1):167–208.

IPCC. 2013. The physical science basis. Contribution of working group I to the fifth assessment report of the intergovernmental panel on climate change. Cambridge, United Kingdom and New York, NY, USA: Cambridge University Press.

Jones, D. S. 1983. Sclerochronology - Reading the record of the molluscan shell. American Scientist 71:384–91.

Jones, D. S., Arthur, M. A., Allard, D. J. 1989. Sclerochronological records of temperature and growth from shells of *Mercenaria mercenaria* from Narragansett Bay, Rhode Island D.S. Marine Biology 102:225–34.

Khim, B. K., Krantz, D. E., Brigham-Grette, J. 2001. Stable isotope profiles of last interglacial (Pelukian Transgression) mollusks and paleoclimate implications in the Bering Strait region. Quaternary Science Reviews 20:463–83.

Khim, B. K, 2001. Stable Isotope profiles of *Serripes groenlandicus* shells. II. Occurrence in Alaskan coastal water in Soutch St. Lawrence Island, northern Bering Sea. Journal of Shellfish Research 20(1):275–81

Khim, B. K. 2002. Stable isotope profiles of *Serripes groenlandicus* shells. I. Seasonal and interannual variations of Alaskan coastal water in the Bering and Chukchi Seas." Geosciences Journal 6(4):257–67.

Khim, B. K., Krantz, D. E., Cooper, L. W., Gerbmeier, J. M. 2003. Seasonal discharge of estuarine freshwater to the western Chukchi Sea shelf identified in stable isotope profiles of mollusk shells. Journal of Geophysical Research 108.

Kilada, R. W., Roddick, D., Mombourquette, K. 2007. Age determination, validation, growth and minimum size of sexual maturity of the Greenland smooth cockle (*Serripes greonlandicus*, Bruguiere, 1789) in eastern Canada. Journal of Shellfish Research 26(2):443–50.

Laudien, J., Brey, T., Arntz, W. E. 2003. Population structure, growth and production of the surf clam *Donax serra* (Bivalvia, Donacidae) on two Namibian sandy beaches. Estuarine, Coastal and Shelf Science 58:105–15.

Laudien, J., 2011. Physical oceanography at time series station Brandal in the Kongsfjorden (Spitsbergen, Arctic), 2009-09 to 2011-06. doi:10.1594/PANGAEA.761660

Laudien, J., 2013. Physical Oceanography at time series station Brandal in the Kongsfjorden (Spitsbergen, Arctic), 2012-09 to 2013-09. doi:10.1594/PANGAEA.819120

Legault, C., Himmelmann, J. 1993. Relation between escape behaviour of benthic marine invertebrates and the risk of psredation. Journal of Experimental Marine Biology and Ecology 170:55–74.

Maclachlan, S. E., Cottier, F. R., Austin, W. E. N., Howe, J. A. 2007. The Salinity : $\delta^{18}O$ Water relationship in Kongsfjorden, western Spitsbergen. Polar Research 26:160–67.

Marchitto, T. M. Jr., Jones, G. A., Goodfriend, G. A., Weidman, C. R. 2000. Precise temporal correlation of holocene mollusk shells using sclerochronology. Quaternary Research 53:236–46.

Miller, G. H., Alley, R. B., Brigham-Grette, J., Fitzpatrick, J. J., Polyak, L., Serreze, M. C., White, J. W. C. 2010. Arctic amplification: Can the past constrain the future? Quaternary Science Reviews 29:1779–90.

Nehrke, G., Nouet, J. 2011. Confocal Raman microscope mapping as a tool to describe different mineral and organic phases at high spatial resolution within marine biogenic carbonates: Case study on *Nerita undata* (Gastropoda, Neritopsina). Biogeosciences 8:3761–69.

Riascos, J., Guzmán, N., Laudien, J., Heilmayer, O., Oliva, M. 2007. Suitability of three stains to mark shells of *Concholepas concholepas* (Gastropoda) and *Mesodesma donacium* (Bivalvia). Journal of Shellfish Research 26(1):43–49.

Richardson, C. A. 2001. Molluscs as archieves of environmental change. Oceanography and Marine Biology, An annual review 39:103–64.

Rogers, J. W. 1993. A History of the Earth. Cambridge: Cambridge University Press.

Romanek, C. S., Grossman, E. L., Morse, J.W. 1992. Carbon isotopic fractionation in synthetic aragonite and calcite: Effects of temperature and precipitation rate. Geochimica et Cosmochimica Acta 56:419–30.

Schauer, U., Fahrbach, E., Osterhus, S., Rohardt, G. 2004. Arctic warming through the Fram Strait: Oceanic heat transport from 3 years of measurements. Journal of Geophysical Research C: Oceans 109:1–14.

Schöne, B. R. 2008. The curse of physiology - challenges and opportunities in the interpretation of Geochemical Data from Mollusk Shells. Geo-Marine Letters 28:269–85.

Schöne, B. R. 2013. *Arctica islandica* (Bivalvia): A unique paleo-environmental archive of the northern north Atlantic Ocean. Global and Planetary Change 111:199–225.

Schöne, B. R., Fiebig, J. 2009. Seasonality in the North Sea during the Allerød and late medieval climate optimum using bivalve sclerochronology. International Journal of Earth Sciences 98:83–98.

Serreze, M. C., Francis, J. 2006. The Arctic on the fast track of change. Weather 61:65–69.

Smith, E., Dent, G. 2005. Modern Raman spectroscopy – a practical approach. John Wiley & Sons, Ltd.

Svendsen, H., Beszczynska-Møller, A., Hagen, J. O., Lefauconnier, B., Tverberg, V., Gerland, S., Ørbæk, J. B., Bischof, K., Papucci, C., Zajaczkowski, M., Azzolini, R., Bruland, O., Wiencke, C., Winther, J. G., Dallmann, W. 2002. The physical environment of Kongsfjorden – Krossfjorden, an Arctic fjord system in Svalbard. Polar Research 21(1):133–66.

Von Bertalanffy, L. 1957. Quantitative laws in metabolism and growth. The Quarterly Review of Biology 32(3):217–31.

Versteegh, E., Blicher, M. E. Mortensen, J., Rysgaard, S., Als, T. D., Wanamaker, A. D. Jr. 2012. Oxygen isotope ratios in the shell of *Mytilus edulis*: Archives of glacier meltwater in Greenland? Biogeosciences 9:5231–41.

Wassenaar, L. I., Brand, U., Terasmae, J. 1988. Isotopic and elemental geochemistry of marine invertebrates from the late Quaternary Fort Langley Formation and Capilano sediments, Southwestern British Columbia, Canada. Chemical Geology: Isotope Geoscience section 73:221–31.

Wegener, A. 1912. Die Entstehung der Kontinente. Geologische Rundschau 3.4:276–92.

Wlodarska-Kowalczuk, M., Pearson, T. 2003. Soft-bottom macrobenthic faunal associations and factors affecting species distributions in an Arctic glacial fjord (Kongsfjord, Spitsbergen). Polar Biology 27:155–67.

Zachos, J. C., Quinn, T. M., Salamy, K. 1996. Deep-sea foraminiferal stable isotope records of the eocene-oligocene climate transition. Paleoceanography 11(3):251.

8 Declaration

Hiermit erkläre ich, dass ich die vorliegende Masterarbeit selbstständig angefertigt habe. Es wurden nur die in der Arbeit ausdrücklich genannten Quellen und Hilfsmittel benutzt. Wörtlich oder sinngemäß übernommenes Gedankengut wurde als solches kenntlich gemacht.

Ort, Datum

Unterschrift der Verfasserin

9 Acknowledgment

Zunächst möchte ich mich bei Prof. Dr. Claudio Richter für die Möglichkeit diese Arbeit in der Arbeitsgruppe Bentho-Pelagische Prozesse zu schreiben bedanken, sowie bei Prof. Dr. Tom Brey für seine Unterstützung bei der Durchführung. Prof. Dr. Gerhard Graf danke ich sowohl für die Übernahme der Erstbetreuung als auch für der Unterstützung in scheinbar ausweglosen Situationen. Dr. Jürgen Laudien möchte ich dafür danken, dass ich diese Arbeit unter seiner Betreuung und mit seiner Unterstützung schreiben durfte. Prof. Dr. Andreas Mackensen und Lisa Schönborn möchte ich dafür danken, dass sie mir die Messung meiner Proben ermöglicht haben und dass trotz streikender Technik am Ende noch alles gut wurde. Dr. Gernot Nehrke danke ich für die Möglichkeit am RAMAN und REM Messungen durchführen zu können und dabei spannende Dinge entdecken zu können. Danke auch an Kerstin Bayer dafür, dass sie mir immer mit Rat und Tat zu Seite gestanden hat. Außerdem danke ich Janina Popp für die tatkräftige Unterstützung im Labor.

Ein großes Dankeschön geht auch an Dr. Lars Beierlein für unglaublich viel fachlichen Input, zahlreiche Stunden der Diskussion und viel viel Motivation. Ich hoffe, ich konnte den Fluch auf dieser Arbeit hiermit brechen!

Ein besonders großer Dank geht auch an Erik Wurz. Für unermüdliches Korrekturlesen und motivieren, für zuhören und diskutieren, mitleiden und mitfreuen.

Zum Schluss möchte ich meiner Familie danken, ohne die das alles gar nicht möglich gewesen wäre.